Materials Horizons

ROYAL SOCIETY OF CHEMISTRY

REVIEW

View Article Online
View Journal | View Issue

Cite this: *Mater. Horiz.*, 2024, **11**, 6257

3D and 4D printing of MXene-based composites: from fundamentals to emerging applications

Ashkan Bigham, [ab] Atefeh Zarepour,[c] Arezoo Khosravi,[d] Siavash Iravani *[e] and Ali Zarrabi *[fg]

The advent of three-dimensional (3D) and four-dimensional (4D) printing technologies has significantly improved the fabrication of advanced materials, with MXene-based composites emerging as a particularly promising class due to their exceptional electrical, mechanical, and chemical properties. This review explores the fundamentals of MXenes and their composites, examining their unique characteristics and the underlying principles of their synthesis and processing. We highlight the transformative potential of 3D and 4D printing techniques in tailoring MXene-based materials for a wide array of applications. In the field of tissue regeneration, MXene composites offer enhanced biocompatibility and mechanical strength, making them ideal for scaffolds and implants. For drug delivery, the high surface area and tunable surface chemistry of MXenes enable precise control over drug release profiles. In energy storage, MXene-based electrodes exhibit superior conductivity and capacity, paving the way for next-generation batteries and supercapacitors. Additionally, the sensitivity and selectivity of MXene composites make them excellent candidates for various (bio)sensing applications, from environmental monitoring to biomedical diagnostics. By integrating the dynamic capabilities of 4D printing, which introduces time-dependent shape transformations, MXene-based composites can further adapt to complex and evolving functional requirements. This review provides a comprehensive overview of the current state of research, identifies key challenges, and discusses future directions for the development and application of 3D and 4D printed MXene-based composites. Through this exploration, we aim to underscore the significant impact of these advanced materials and technologies on diverse scientific and industrial fields.

Received 11th August 2024,
Accepted 30th August 2024

DOI: 10.1039/d4mh01056f

rsc.li/materials-horizons

Wider impact

This review highlights the developments in the 3D/4D printing of MXene-based composites, focusing on their processing and emerging applications. The integration of MXenes with advanced printing technologies has led to significant advancements in creating materials with superior electrical, mechanical, and chemical properties. These developments are of significant wider interest due to the transformative potential of MXene-based composites in various high-impact fields. In biomedical applications, MXene-based scaffolds and implants offer enhanced biocompatibility and mechanical strength, while in drug delivery, their high surface area and tunable chemistry enable precise control over therapeutic release. In energy storage, MXene electrodes provide exceptional conductivity and capacity, essential for next-generation batteries and supercapacitors. Additionally, their sensitivity and selectivity make them ideal for environmental and biomedical sensing applications. The future of this field holds immense promise, with the dynamic capabilities of 4D printing enabling materials that can adapt to changing conditions and functional requirements. The insights provided in this review will help shape materials science by guiding future research towards optimizing MXene composites for specific applications, addressing current challenges, and exploring new frontiers. This will ultimately lead to the development of smarter, more efficient, and highly functional materials that can meet the evolving demands of various industries.

[a] *Institute of Polymers, Composites, and Biomaterials, National Research Council (IPCB-CNR), Naples 80125, Italy*
[b] *Department of Chemical, Materials and Production Engineering, University of Naples Federico II, Piazzale V. Tecchio 80, 80125 Naples, Italy*
[c] *Department of Research Analytics, Saveetha Dental College and Hospitals, Saveetha Institute of Medical and Technical Sciences, Saveetha University, Chennai 600 077, India*
[d] *Department of Genetics and Bioengineering, Faculty of Engineering and Natural Sciences, Istanbul Okan University, Istanbul 34959, Turkey*
[e] *Independent Researcher, W Nazar ST, Boostan Ave, Isfahan, Iran. E-mail: siavashira@gmail.com*
[f] *Department of Biomedical Engineering, Faculty of Engineering and Natural Sciences, Istinye University, Istanbul 34396, Turkey. E-mail: alizarrabi@gmail.com*
[g] *Graduate School of Biotechnology and Bioengineering, Yuan Ze University, Taoyuan 320315, Taiwan*

1. Introduction

In recent years, the field of additive manufacturing has witnessed significant advancements with the emergence of three-dimensional (3D) and four-dimensional (4D) printing technologies. These innovative techniques have developed the way of designing materials, paving the way for novel applications across various industries.[1–3] 3D-printing is a technique for the production of 3D objects by building up material in layers according to a digital design that enables producing lightweight constructions with intricate designs in little time with lower risk and enhanced accessibility.[4,5] In here, materials are used as viscoelastic ink that is extruded through a deposition nozzle in a layer-by-layer manner to create scaffolds and other 3D shapes on a computer-controlled translation stage.[6] There are different methods for the 3D printing (Fig. 1) of materials including polyJet printing, fused deposition modeling (FDM), stereolithography (SLA), selective laser sintering (SLS), multi-jet fusion printing, direct metal laser sintering (DMLS), electron beam melting (EBM), and digital light process (DLP); each of them has its specific features and are described in detail in other papers.[7] Moreover, 4D printing was introduced to integrate a product's schematic into a pliant, smart material through a conventional 3D printer.[8] The item can metamorphose or be reshaped into the intended layout by exposing it to specific stimuli like heat, moisture, pressure, pH, light, *etc.* Essentially, 4D printing signifies a progression from 3D printing technology by enabling the creation of dynamic objects. Additive manufacturing employs 3D printers for crafting 3D models; nonetheless, it has limitations in generating static products with confined build sizes. To combat these constraints, the concept of 4D printing emerged, enabling the conversion of 1D or 2D filaments into pre-set 3D forms and with the capacity to transition across dimensions.[3,8,9]

MXenes, which were discovered in 2011, have garnered significant attention in the scientific community due to their exceptional properties and diverse applications. These materials exhibit a unique combination of metallic conductivity, mechanical strength, and hydrophilicity, making them highly versatile for various fields ranging from energy storage to catalysis.[12–14]

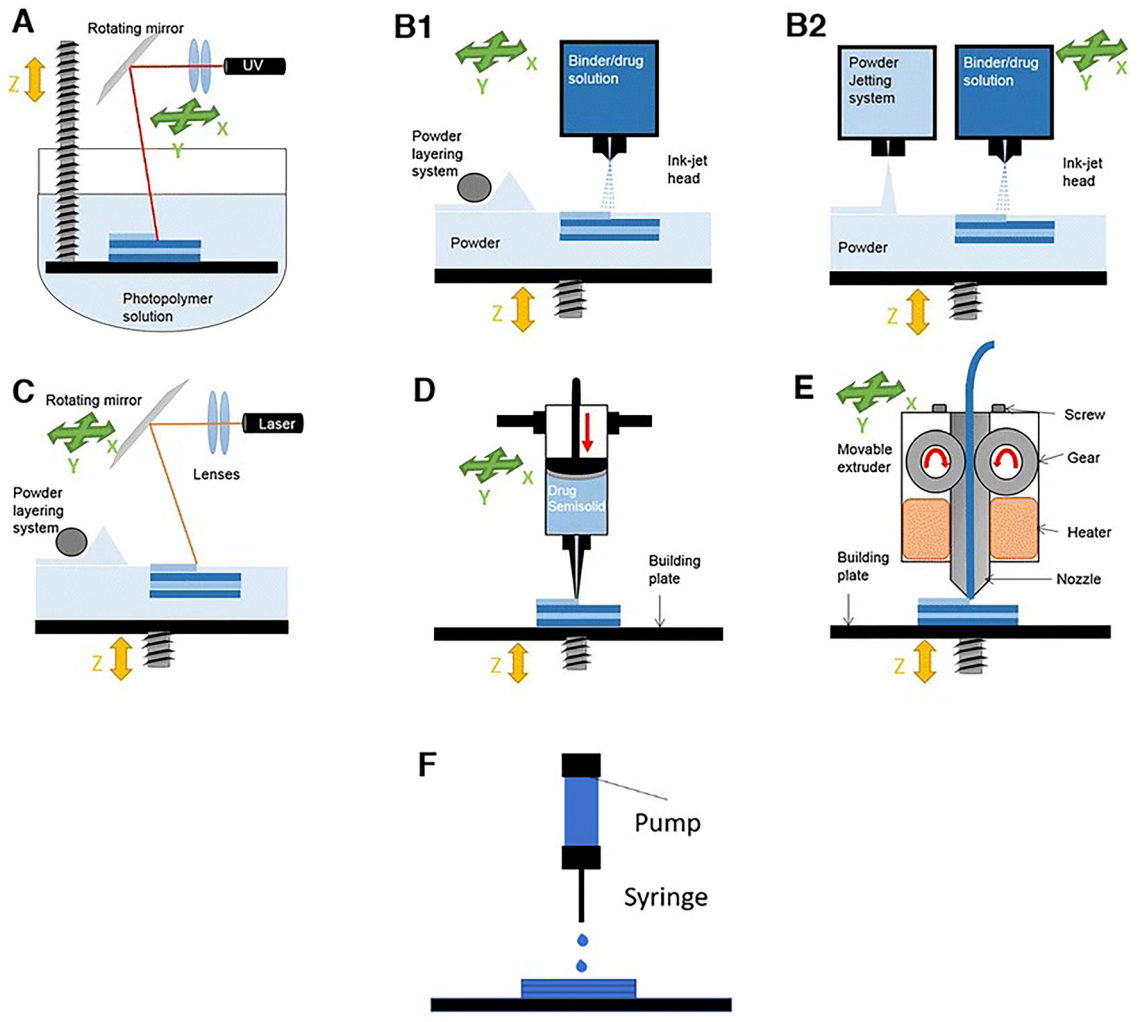

Fig. 1 Some of the different types of 3D printing methods including stereolithography (SLA) (A), powder bed and powder jetting (B1 and B2), selective laser sintering (SLS) (C), semi-solid extrusion (EXT) (D), fused deposition modelling (FDM) (E), and direct ink writing (DIW) (F). (A)–(E) Reprinted with permission from ref. 10. Copyright 2016, Springer Nature. (F) Reprinted from ref. 11 under the terms of the Creative Commons Attribution License. Copyright 2021, Wiley.

MXenes are a class of two-dimensional (2D) transition metal carbides, nitrides, or carbonitrides with the general formula $M_{n+1}X_nT_x$, where M is an early transition metal (such as Ti, V, Nb, or Mo), X is carbon and/or nitrogen, T represents surface terminations (such as hydroxyl, oxygen, or fluorine), and n is the number of transition metal layers. The unique structure of MXenes consists of alternating layers of transition metals and carbon/nitrogen atoms, with the surface functional groups providing stability and tunable properties.[15–18] The synthesis of MXenes typically involves the selective etching of the 'A' element from MAX phases, which are layered ternary carbides or nitrides. This etching process exposes the 2D layers of transition metals and carbon/nitrogen atoms, resulting in MXene nanosheets. The choice of transition metal, surface termination, and etching conditions can be tailored to control the properties of MXenes for specific applications.[19,20]

The layered structure of MXenes imparts exceptional properties, such as high electrical conductivity, mechanical strength, and chemical stability. These properties make MXenes highly attractive for a wide range of applications, including energy storage, catalysis, sensors, and electromagnetic shielding.[16,21–23] The ability to functionalize the surface of MXene nanosheets further enhances their versatility and compatibility with various matrices; the surface functionalization of MXene nanosheets with hydrophilic groups enhances their dispersibility in solvents and compatibility with polymer matrices.[24,25] One of the key advantages of MXenes is their high surface area, which enables efficient ion intercalation and rapid charge transfer. This property makes MXene composites ideal for application in supercapacitors, batteries, and electrochemical sensors.[26–28] Additionally, MXenes exhibit excellent mechanical properties, allowing them to enhance the strength and toughness of polymer composites when incorporated as fillers.[29,30] Moreover, MXenes have shown great potential in catalysis due to their tunable surface chemistry and catalytic activity. By tailoring the surface functional groups of MXene nanosheets, researchers can design catalysts with enhanced selectivity and efficiency for various chemical reactions.[31–33]

One particularly exciting area of research involves the integration of MXene-based composites into the 3D and 4D printing processes, with immense potential for various applications.[34,35] From flexible electronics to biomedical devices, MXene-based structures exhibit unparalleled versatility and performance. The advancement of novel MXene-based materials in 3D printing presents exciting prospects for progress in additive manufacturing technologies, particularly in the realm of 4D printing.[36,37] The integration of innovative materials, like shape memory polymers and composites, has played a crucial role in the development of 4D printing. These materials enable the creation of smart structures that can self-assemble, self-repair, or adapt to different environments autonomously.[38] The potential applications of 4D printing are vast, ranging from self-folding furniture to adaptive camouflage in military settings.[39–41] By introducing cutting-edge shape memory polymer composites (SMPCs), printed components can now possess enhanced functionalities, such as the capability to alter their shape, functioning as intelligent actuators responsive to external stimuli. These materials have captured significant attention for the advancement of soft robotic systems that can be produced rapidly and cost-effectively.[37]

The 3D/4D printing of advanced MXene-based materials offers numerous advantages, including enhanced mechanical properties, electrical conductivity, and chemical stability.[42] However, challenges remain in optimizing the dispersion of MXene nanosheets within printing matrices, ensuring uniformity in printed structures, and scaling up production for industrial applications. Addressing these challenges will be crucial for realizing the full potential of MXene-based materials in additive manufacturing.[40,43,44] The purpose of this review is to provide a comprehensive overview of the current state-of-the-art technologies, advancements, challenges, and future perspectives in the field of additive manufacturing using MXene-based 3D/4D printed materials. By exploring the unique properties of MXenes, the capabilities of 3D and 4D printing technologies, and the emerging applications of MXene composites across various industries, this review aims to shed light on the transformative potential of these materials in shaping the future of advanced manufacturing. Through a critical analysis of the opportunities, limitations, and key research directions in the field, we seek to inspire further innovation and exploration in leveraging MXenes and their composites for creating intelligent, adaptive, and high-performance materials for diverse applications, from biomedicine to electronics and beyond.

2. 3D/4D printing of MXene-based materials

2.1. 3D printing

Utilizing 3D printing has enhanced across various industries, with a projected increase in its widespread adoption both commercially and among the general public.[40] Its efficacy stems from the amalgamation of an intuitive design phase facilitated by user-friendly software and flexible, uncomplicated printing procedures. Expanding the array of printable materials to encompass deformable and stimuli-responsive variants holds the promise of propelling the 3D printing domain to greater prominence and relevance. In the near future, this diversification is poised to facilitate the production of readily deployable piezoresistive sensors and dynamic structures capable of undergoing programmed transformations post-stimulus activation, akin to the characteristics of 4D printing materials. Concurrently, integrating these intelligent materials with nanomaterials has the potential to enhance their dynamic responsiveness and introduce novel functionalities. This synergistic approach opens avenues for innovation and advancement in the realm of additive manufacturing, paving the way for the creation of cutting-edge products with enhanced capabilities and adaptability.[40]

Digital light processing (DLP) 3D printing technology is a type of additive manufacturing that utilizes light to cure liquid photopolymer resins layer by layer, ultimately creating a solid object.[45] In DLP printers, a light source, often a projector,

shines light onto a resin tank containing the liquid photopolymer. The light exposure causes the resin to harden or cure, forming a thin layer of the object being printed. One of the key advantages of DLP technology is its speed compared to other 3D printing methods. Since the entire layer is exposed to light simultaneously, DLP printers can produce objects faster than traditional methods like fused deposition modeling (FDM). Additionally, DLP printing can achieve high levels of detail and accuracy, making it suitable for applications requiring intricate designs or fine features. However, DLP printing also has its limitations. The layer thickness in DLP printing is typically larger than in other technologies, which can affect surface finish and resolution. Post-processing steps such as cleaning and curing are often necessary to achieve the desired final quality. In one study, the synthesis of 3D printable photocurable resins incorporating $Ti_3C_2T_z$-MXenes with their exceptional electrical properties was documented.[34] Formulation of stable inks suitable for digital light processing 3D printing technology was achieved, enabling the production of intricate 3D composite structures with precise printing accuracy. To improve the material's electrical conductivity, annealing processes were conducted, followed by a comprehensive analysis of the resulting materials. The findings demonstrated the successful creation of objects with enhanced electrical conductivity, paving the way for advancements in the realm of 3D electronic development.[34]

Some 3D printing methods, including fused deposition modeling (FDM), stereolithography (SLA), and selective laser sintering (SLS), have been adapted to accommodate MXene-based materials.[46–48] These techniques enable the layer-by-layer deposition of MXene-infused filaments or resins, allowing for the precise fabrication of intricate geometries. The high electrical conductivity of MXenes makes them ideal candidates for application in electronics, sensors, and energy storage devices produced using 3D printing technologies.[49,50] FDM is a widely used 3D printing technique that involves the extrusion of thermoplastic filaments through a heated nozzle. In the context of MXene-based materials, FDM can be employed to fabricate functional prototypes and components with improved mechanical strength and conductivity. Controlling the deposition parameters and material composition is crucial for achieving optimal results. In one study, a novel MXene/recycled carbon fiber (rCF) reinforced PLA 3D printing material was synthesized *via* the electrostatic self-assembly method of MXenes and recycled carbon fiber.[46] The incorporation of MXenes played a pivotal role in bolstering the bonding at the fiber–substrate interface within the reinforced PLA filaments. Consequently, the printed components exhibited a notable improvement in toughness, with the flexural strength reaching 105.45 MPa, modulus at 5.98 GPa, and a notched impact strength of 7.12 kJ m^{-2}. These enhancements displayed a substantial increase of 15.6%, 112.1%, and 31.8%, respectively, compared to pure PLA materials. Furthermore, the modified PLA material showcased superior electromagnetic shielding performance primarily driven by absorption mechanisms.[46] This study not only presents a practical method for enhancing recycled carbon fiber-reinforced thermoplastic PLA but also offers valuable insights into the design of sustainable composites that are structurally robust and functionally integrated. By leveraging the synergistic effects of MXenes and recycled carbon fiber, this research contributed to the development of high-performance, environmentally conscious materials for advanced applications in additive manufacturing and beyond.

Stereolithography (SLA) is a resin-based 3D printing technique that uses ultraviolet (UV) light to solidify liquid photopolymer resins layer by layer. This high-resolution printing method is suitable for producing intricate MXene-based structures with fine details and smooth surfaces. Proper resin selection and curing parameters are essential for maximizing the mechanical and electrical properties of the printed objects.[47] The utilization of stereolithographic 3D printing has gained momentum for the rapid fabrication of intricately designed gels with unique 3D structures. In one study, MXene ($Ti_3C_2T_x$) was introduced for the first time as a versatile photo blocker in a photo-curable aqueous ink utilized in a novel stereolithography technology known as continuous liquid interface production (CLIP).[47] This innovative approach aimed to facilitate the production of hydrogels with intricate geometries. By acting as an efficient photo blocker, MXene nanosheets played a crucial role in significantly reducing light scattering within the hydrogel precursor ink during the CLIP printing process, thereby enhancing printing precision. Subsequent transformation through solvent exchange with glycerin resulted in the creation of an organogel with exceptional adhesive properties towards diverse surfaces, showcasing its potential as an adhesive sensor capable of detecting various body movements. Moreover, the CLIP-printed organogel exhibited promising applications in atmospheric water harvesting, leveraging the innate hygroscopic nature of the organogel and the excellent light-to-heat conversion performance facilitated by MXene nanosheets. Additionally, the CLIP-printed hollow organogel demonstrated enhanced efficiency due to its larger surface area.[47] These findings underscored the multifunctional capabilities of MXenes as an additive for CLIP inks, hinting at the emergence of new avenues for 3D printing advanced devices with enhanced functionalities and performance metrics.

Selective laser sintering (SLS) is a powder-based 3D printing technology that utilizes a high-powered laser to sinter powdered materials, such as polymers or metals, into solid objects. In the case of MXene composites, SLS can be used to create functional parts with enhanced strength and conductivity. Optimizing the sintering process and powder composition is critical for achieving the desired material properties.[48] In a recent investigation, the synthesis of MXene (Ti_3C_2) was reported on the surface of a metal–organic framework (HKUST-1) to form a composite with polyamide 12 (PA12).[48] This composite exhibited notable enhancement in both mechanical strength and fire safety characteristics. The assessment of the PA12 composite reinforced with MXene-on-HKUST-1 unveiled substantial reductions in total heat release (by 18.5%), peak heat release (by 26.1%), and total smoke emission (by 28.1%). Additionally, the incorporation of MXene-on-HKUST-1 led to improvements in tensile strength and

dynamic mechanical properties. These results provided insights into the underlying mechanisms responsible for the enhancement of mechanical strength and flame-retardant capabilities conferred by MXene-on-HKUST-1.[48] By leveraging selective laser sintering, this research introduced a promising technology for the advancement of high-performance MXene-reinforced PA12-based flame-retardant composites. The successful integration of MXene onto HKUST-1 opens up new avenues for the development of polymeric materials with enhanced flame resistance and mechanical robustness, catering to the evolving needs of various industrial applications.

From healthcare to electronics, the utilization of MXenes in 3D printing opens up new avenues for innovation and customization. In the field of healthcare, 3D printing of MXene composites (Fig. 2) finds application in the production of patient-specific implants and prosthetics, tissue engineering, cancer therapy, and drug delivery systems.[51] The biocompatibility and mechanical strength of MXenes make them ideal candidates for creating personalized medical devices that offer superior performance and durability.[52–54] In the realm of electronics, MXene-based composites hold promise for developing next-generation components with enhanced conductivity and thermal management.[55–57] By leveraging the precision of 3D printing technology, engineers can fabricate intricate circuitry, sensors, and energy storage devices that exhibit superior performance and reliability. Moreover, the aerospace and automotive industries stand to benefit from the applications of 3D printing of MXenes and their composites. The lightweight nature and exceptional mechanical properties of MXenes make them ideal for producing high-performance structural components, such as aircraft parts or automotive components, with reduced weight and increased strength.[30] In the field of energy storage, MXenes and their composites offer groundbreaking potential for improving the performance and efficiency of batteries and supercapacitors.[58–60] These advanced materials, known for their high conductivity and large surface area, are poised to address the growing demand for energy storage solutions in various industries. One key application of MXenes in energy storage is their use in lithium-ion batteries.[61–63] By incorporating MXene composites as electrode materials, researchers aim to enhance the energy density, charge/discharge rates, and cycling stability of batteries. This can lead to the development of longer-lasting and faster-charging batteries for electric vehicles, portable electronics, and renewable energy systems.[64,65] Moreover, MXene-based materials show promise in supercapacitors, which are crucial for rapid energy storage and release applications.[66] Indeed, the integration of MXene-based materials in supercapacitors represents a significant leap in energy storage technology, offering high conductivity, exceptional capacitance, and rapid charge–discharge cycles. The high surface area and excellent electrical conductivity of MXenes make them ideal candidates for improving the energy storage capacity and efficiency of supercapacitors. This provides the capability of quick charging times and high-power output in devices requiring rapid energy bursts. Furthermore, the versatility of MXenes allows for the customization of energy storage devices to meet specific application requirements. By tuning the composition and structure of MXene composites, researchers can tailor the performance characteristics of batteries and supercapacitors for different applications, ranging from grid-scale energy storage to wearable electronics.[67,68] Leveraging the versatility of 3D printing techniques in this domain holds immense promise for the fabrication of customized and efficient supercapacitor devices.[69] By harnessing the precision and flexibility of 3D printing, researchers can tailor the design and structure of supercapacitors to maximize performance while minimizing size and weight. The additive manufacturing process enables the creation of intricate electrode architectures that optimize the utilization of MXene's impressive electrochemical properties.[70] Furthermore, the use of 3D printing allows for the seamless integration of MXene-based electrodes into complex device configurations, enhancing overall energy storage capacity and efficiency. This approach paves the way for the development of lightweight and compact supercapacitors with enhanced power density and longevity.[69,71] The marriage of 3D printing technology with MXene-based supercapacitors not only streamlines the manufacturing process but also facilitates the development of innovative energy storage solutions tailored to specific application requirements. For instance, quasi-solid-state symmetrical

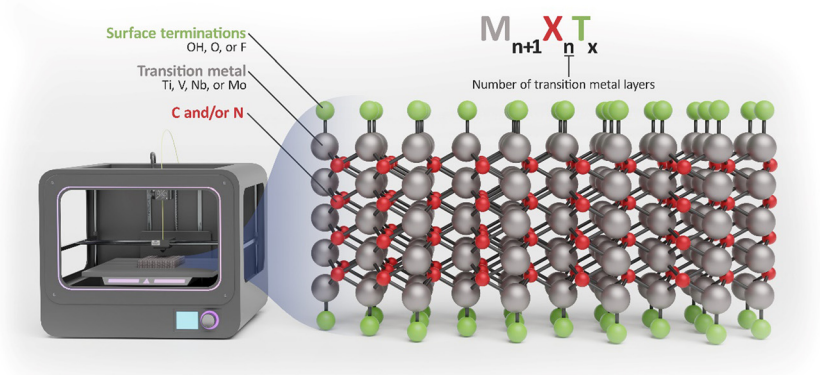

Fig. 2 Application of the 3D-printing method for fabricating MXenes.

micro-supercapacitors (MSCs) were prepared using direct 3D printing with aqueous MXene sediment ink devoid of additives.[71] Traditionally, the MXene sediment, predominantly comprising multi-layered MXene and un-etched MAX, was discarded following the collection of d-$Ti_3C_2T_x$ suspension. However, this research demonstrated a paradigm shift by utilizing the MXene sediments in the ink to modulate viscoelastic properties, enabling the printing of MSCs with diverse structures on substrates at room temperature *via* direct ink writing technology. The investigation unveiled that the 3D-printed MSCs exhibited commendable charge storage capabilities, showcasing a peak areal capacitance of 2.337 F cm^{-2} at 2 mV s^{-1}, an areal energy density of 207.81 μW h cm^{-2}, a power density of 3.74 mW cm^{-2}, and capacitance retention exceeding 93.1% after 10 000 cycles. By utilizing a waste-free MXene ink in conjunction with 3D printing technology, this approach offered a promising avenue for producing the next generation of portable and wearable electronic devices. The combination of MXene ink recycling and 3D printing not only enhanced the sustainability of energy storage device fabrication but also unlocked new possibilities for designing high-performance micro-supercapacitors tailored for compact and efficient electronic applications.[71] This research underscores the potential of integrating MXene-based materials and additive manufacturing techniques in advancing energy storage solutions for the evolving landscape of portable electronics and wearable technology. As research in this field progresses, we can anticipate the emergence of next-generation supercapacitors that offer superior performance, reliability, and sustainability, driving advancements in diverse sectors ranging from electronics to renewable energy systems.

2.2. 4D printing

Incorporating MXenes into composites for 4D printing opens up a realm of possibilities in the field of advanced manufacturing. By incorporating stimuli-responsive polymers or shape-memory alloys with MXene-based materials, researchers can create structures that exhibit programmable shape-changing behaviors. This capability opens up new avenues for the design of smart materials and adaptive structures for diverse applications, including soft robotics and biomedical devices.[72] When discussing the 4D printing of MXenes and their composites, it is essential to delve into the unique properties and applications of these innovative materials. One key aspect to explore is the dynamic capabilities of 4D printing, where printed objects can change shape or function in response to external stimuli.[72] By integrating MXenes into these composites, researchers aim to enhance the responsiveness and adaptability of printed structures. This can lead to the development of smart materials that exhibit self-healing, shape memory, or tunable mechanical properties.[37] In the undertaken study, a SMPC was manufactured and assessed using a pure thermoplastic polyurethane (TPU):polylactide acid (PLA) polymer blend system integrated with embedded MXene (Ti_3C_2) flakes. The mechanical, thermal, and morphological characteristics demonstrated substantial enhancements with the inclusion of 0.5 wt% MXene. With higher loadings of 2 wt% MXene, the composite exhibited exceptional shape memory effects, achieving rapid recovery to nearly 98% of its original position in less than 14 seconds. The rheological behavior and thermal properties were scrutinized, succeeded by 3D printing utilizing material extrusion. The findings underscored the significant potential of MXene-infused composites for swift shape memory actuation in 3D/4D printed architectures. Several printed designs exemplify the considerable deformations suitable for deployable structures.[37] Furthermore, the use of MXene-based composites in 4D printing holds promise for various applications, ranging from biomedical devices to aerospace components. The ability to precisely control the microstructure and properties of printed objects allows for tailored solutions in different industries. For instance, MXene composites could be utilized in the creation of sensors, actuators, or even soft robotics with unprecedented functionalities.[73,74]

When comparing 3D and 4D printing of MXene-based composites, several key differences emerge that influence their applications and capabilities in advanced manufacturing processes.[75] Understanding these distinctions is essential for harnessing the full potential of MXene materials in additive manufacturing. 3D printing involves the layer-by-layer deposition of materials to create 3D objects. In the context of MXenes, 3D printing allows for the fabrication of complex structures with precise geometries and tailored properties. This technology is widely used in various industries for rapid prototyping, custom manufacturing, and production of intricate parts.[76] On the other hand, 4D printing introduces an additional dimension of adaptability and responsiveness to printed objects. In 4D printing of MXene-based composites, the materials are designed to exhibit dynamic behaviors in response to external stimuli, such as temperature changes, light exposure, or mechanical stress. This enables the printed structures to change shape, properties, or functionality over time.[75] One of the main differences between 3D and 4D printing lies in the static *versus* dynamic nature of the printed objects. While 3D-printed MXene composites result in fixed structures with predetermined properties, 4D printing introduces the concept of programmable materials that can self-transform or self-assemble in a controlled manner. This opens up new possibilities for creating smart materials and adaptive devices.[77]

The inception of 4D printing marks a significant evolution in additive manufacturing, introducing the temporal dimension into the established realm of 3D printing technologies.[78] By integrating the dimension of time, 4D printing empowers structures to dynamically transform and adapt in response to various stimuli, including light, heat, magnetism, electricity, solvent, and pH, among others. This transformative capability is enabled by smart materials like shape memory polymers, alloys, hydrogels, ceramics, and composites that exhibit responsive properties. In contrast to traditional 3D printing, the dynamic alterations in structure and properties rendered by 4D printing unlock a myriad of applications across sectors such as aerospace, biomedical, soft robotics, engineering, and fashion. The versatility of 4D printed materials holds the potential to develop the manufacturing industry by introducing

adaptable and customizable components that can self-modify based on environmental triggers. The advent of 4D printing heralds a new era of innovation, where materials no longer remain static but evolve over time to meet changing requirements. This paradigm shift towards dynamic and responsive fabrication techniques not only expands the horizons of design possibilities but also paves the way for enhanced functionality and efficiency in a wide range of industrial applications, promising transformative advancements in the landscape of manufacturing and beyond.[78,79]

3. Emerging applications

3.1. Smart sensors and (bio)sensing systems

Recently, there has been a progressive development in advanced materials and manufacturing techniques both of which led to a revolution in the field of sensing systems.[80] Integrating MXenes and related composites with additive manufacturing was synchronized with the creation of smart sensing platforms.[81,82] MXenes are attributed to 2D nanomaterials made of transition metal nitrides, carbides, and carbonitrides. MXenes have received considerable attention owing to their excellent properties for various applications – electronics, biomedicine, mechanical, chemical, *etc.*[83,84] In this section, recent progress made in the sensing systems of MXene composites manufactured through 3D and 4D printing is covered (Table 1).

Pressure sensors are able to determine the force being applied on their surface by a fluid like gas or liquid. They convert the applied force into electrical signals which then become readable to electronic devices. Pressure sensors are being extensively used in different applications including healthcare, aerospace, *etc.*[92] A MXene-based system was fabricated through 3D printing as a flexible and wearable sensor for real-time tracking of biosignals (Fig. 3(A)). For the printing step, different concentrations of size selected MXene flakes were dissolved in water to fabricate inks, with different viscosity, which were then printed on a styrene–ethylene–butylene–styrene (SEBS) substrate. The carbon backbone of MXene provided the capability of electrical conduction and high flexibility and the presence of several negatively charged terminal groups on its surface introduced it as an ideal triboelectric compound. This sensor had high sensitivity and contained triboelectric nanogenerators, which were power-efficient. MXene particles ($Ti_3C_2T_x$) with excellent conductivity and triboelectric properties were applied as both conducting and triboelectrification layers for pressure sensors and triboelectric nanogenerators, respectively. The combination of MXene particles with the SEBS polymer matrix, which was skin-like, led to a highly flexible sensing platform with a positive triboelectric property. Without the need for an external power source, the platform could continuously monitor radial artery pulse waveform with a detection limit as low as 9 Pa and a sensitivity of 6 kPa^{-1}. The power of the physiological biosignal monitoring system was fully supplied by human motion.[85] So far, various flexible pressure sensors based on different sensing mechanisms have been designed and developed, such as piezoelectric sensors, piezoresistive sensors, electrical sensors, *etc.*[93–95] Among them, piezoresistive sensors have attracted considerable attention owing to some prominent advantages—easy-to-prepare procedure, low cost, fast signal attainment, *etc.*[96] *Via* fused deposition molding, a four-component composite consisting of polyurethane, $Ti_3C_2T_x$, manganese ferrite, and multi-walled carbon nanotubes was designed with a Voronoi structure. The combination of 0, 1, and 2D nanofillers including electrostatic bonding of the MXene and manganese ferrite nanoparticles followed by the addition of carbon nanotubes led to the homogeneous dispersion of nanofillers and subsequently superb conductivity. The mechanical properties of the platform were satisfactory with a gauge factor in the range of 1.33–3.73 and a cyclic compression of 6000 s indicating the good durability of this system. The pressure sensor designed in this study was highly sensitive to human motion with less weight compared to similar intelligent sensors that are used for electromagnetic shielding applications.[86] An ultralight 3D scaffold was fabricated through additive manufacturing as a piezoresistive sensor (Fig. 3(B)). First, a polymer-based 3D-printed scaffold with gyroid lattices was manufactured with a stereolithography 3D printer followed by dip coating of the scaffolds in the MXene sheet solution. Finally, the surface-coated scaffolds were exposed to heat treatment at 450 °C for 3 h under nitrogen to get rid of the polymer. It turned out that the compressive strength of MXene-based scaffolds was 27.18 kPa with a thermal conductivity of 0.3454 W m^{-1} K^{-1} which could go up as high as 23.88 W m^{-1} K^{-1}. The structure of the scaffold including gyroidal and porous structure with high electrical conductivity of MXene sheets ($Ti_3C_2T_x$) makes it a promising candidate for high-performance sensing applications.[97]

In recent years, rapid advancements have been made in flexible and wearable sensors with extended applications. One of those areas is agriculture, and an electronic flexible sensor can facilitate effective and constant interfacing with the surface of a plant for monitoring parameters related to the abiotic environment.[98] Tracking and detection of ethylene as a well-known phytohormone are of particular interest because of its important role in plant growth, immunity, senescence, and development. By determining the ethylene emission, it is possible to anticipate the ripening time followed by harvesting of the crops. This is especially the case for fruits which require an appropriate time to harvest, preventing food waste.[99] Plant wearable sensors were designed and manufactured from MXene-reduced palladium nanoparticles for continuous and *in situ* detection of ethylene. The sensors consisted of radio-frequency antennas and gas sensors both of which collaborate enabling wireless readout and better perception of received information. Applying MXene-reduced palladium nanoparticles was advantageous in terms of ethylene response and led to 1.16% improved ethylene response at 1 ppm and the limit of detection was 0.084 ppm. The sensor tags were tested and attached onto the surface of the leaf and fruit and could measure the emitted ethylene with high precision compared to gas chromatography-mass spectrometry, used as a reference method.[87]

Table 1 Various MXene-based 3D printed platforms for different applications

Composition	Application	Physicochemical properties	Fabrication method	Remarks	Ref.
$Ti_3C_2T_x$-coated styrene–ethylenebutylene–styrene	Pressure sensing	Power output: 816.6 mW m^{-2} Sensitivity: 6.03 kPa^{-1} Detection limit: 9 Pa Response time: 80 ms	3D extrusion printing	– Fabrication of a self-powered and flexible wearable device with the ability of real-time monitoring physiological biosignals – Ability of monitoring radial artery pulse – Improving the conductivity of the composite as well as tuning its viscoelastic property for 3D printing resulted from the incorporation of MXene nanosheets	85
Polyurethane/$Ti_3C_2T_x$/$MnFe_2O_4$/multi-walled carbon nanotubes	Pressure sensing	Gauge factor: 1.33–3.73 Sensing compression range: 89% strain with 12.03 MPa stress Durability: 6000 s (cyclic compression)	Fused deposition molding printing	– Fabrication of a thermoplastic composite with a superb conductive structure *via* the fused deposition modeling technique using a parametric Voronoi structure – A type of pressure sensor which is suitable for monitoring human motion such as finger bending, wrist bending, *etc.*	86
MXene-reduced palladium nanoparticles	Wireless plant wearable ethylene sensor	Electrical conductivity: $\approx$30 000 S m^{-1} 1.16% ethylene response at 1 ppm with 0.084 ppm limit of detection	Direct screen printing	– Fabrication of plant wearable sensor tags using $Ti_3C_2T_x$ MXene nanosheets modified with palladium nanoparticles – The ethylene response was 1.16% at 1 ppm exhibiting the high potential of these tags for *in situ* fruit freshness evaluation and precision agriculture	87
$Ti_3C_2T_x$ flakes	Energy storage	Areal capacitance: $\sim$1035 mF cm^{-2} Energy density: 51.7 μW h cm^{-2}	Extrusion printing	– Fabrication of a micro-supercapacitor for energy storage applications – Utilizing additive-free ink method with desirable viscoelastic behavior provides the capability of printing at room temperature with high potential for scale-up production – Exhibiting exceptional electrochemical performance as well as high areal capacitance	88
MXene ($Ti_3C_2T_x$)-based micro-supercapacitors	Energy storage	Areal capacitance: 1.1 F cm^{-2} Energy density: 154 μW h cm^{-2}	Direct screen printing	– Fabrication of a multifunctional aqueous printable MXene ink for energy storage applications that could be deposited on different substrates – Exhibiting exceptional sensitivity to body movements and a fast response of 35 ms	89
Ti_3C_2 nanosheets-*N*-isopropylacrylamide (NIPAM)-alginate	Skin flap regeneration	—	Microfluidic-integrated extrusion-based 3D printing	– Introducing a multifunctional scaffold for skin flap regeneration application – Exhibiting thermos-responsive ability resulting from the presence of MXene in the structure of the scaffold that provided the capability of high photothermal conversion followed by control over the swelling/shrinkage of the structure – Accelerating the proliferation and migration of endothelial cells due to the faster release of vascular endothelial growth factor in response to near-infrared (NIR) irradiation	90
Ti_3C_2 nanosheets-berberine-biphasic calcium phosphate-sodium alginate	Bone infection therapy and regeneration	—	Extrusion printing	– Fabrication of a composite scaffold for bone infection and regeneration – Elimination of bacterial infection due to the presence of MXene nanosheets with the ability of photothermal conversion – Enhancing berberine release in response to irradiation that enhanced the antibacterial effect and promoted cell viability and proliferation	91

Manufacturing of 3D-printed flexible electronics comes with some challenges including low printing resolution and precision, complicated ink formulations, *etc.* High-performance flexible wireless electronics were fabricated through direct printing at room temperature; at first, an additive-free MXene aqueous ink with suitable rheological properties was prepared through a modified minimally intensive layer delamination route and it turned out excellent leading to high-precision printing—conductivity: 6900 S cm^{-1} and 3 μm ultra-narrow line gap, with a high spatial uniformity. Concentrated $Ti_3C_2T_x$ MXene aqueous inks ($\sim$60 mg mL^{-1}) containing ultrathin single-layer flakes were prepared in which the average size and thickness of flakes were $\sim$1.6 μm and $\sim$1.5 nm, respectively. The fabricated inks exhibited suitable shear-thinning

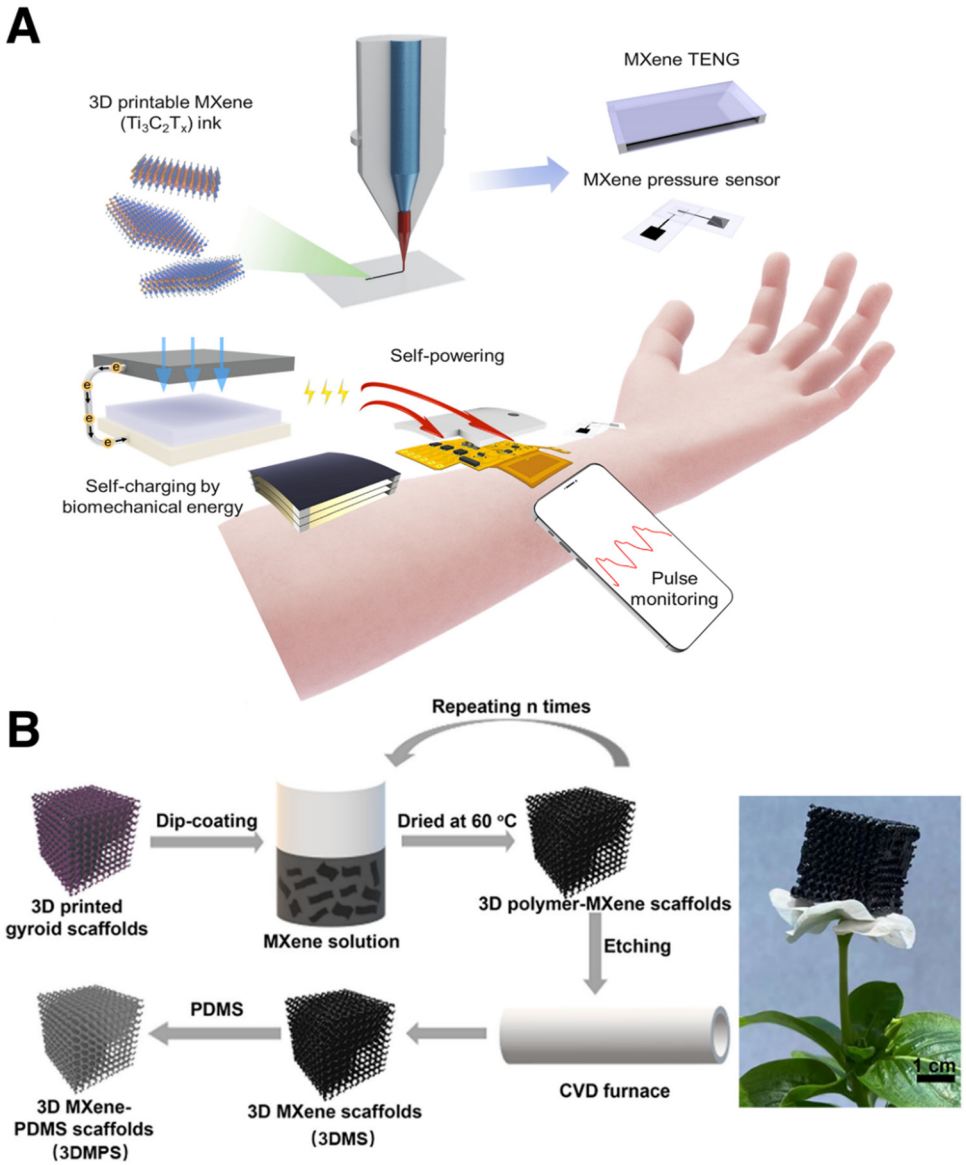

Fig. 3 MXene-based 3D printed platforms as pressure sensors. (A) Schematic illustration of the fabrication process of a self-powered wearable sensor for real-time monitoring of physiological biosignals. Reprinted with permission from ref. 85. Copyright 2022, Elsevier. (B) Preparation steps of ultralight 3D printed gyroid scaffolds made of polydimethylsiloxane which underwent surface modification and coating with MXene nanosheets as a piezoresistive sensor. Reprinted from ref. 97 under the terms of the Creative Commons CC BY license. Copyright 2022, Wiley. Abbreviations: TENG, triboelectric nanogenerators; PDMS, polydimethylsiloxane; 3DMS, 3D MXene scaffold; 3DMPS, 3D MXene polymer scaffold.

viscoelastic behaviors owing to the high concentration of the inks with a large single-layer ratio (>90%) and a narrow size distribution which led to a continuous extrusion followed by fast solidification. The interesting point is that the inks were stored under protected conditions—argon gas and darkness to protect the flakes against oxidation at low temperatures—for two years for potential ink printing. The sensor was tested in different manners and could simultaneously work in wireless power harvesting, T/H sensing, and data transmission (Fig. 4).[100]

Other types of MXene-based 3D printed structures have been designed for various sensing applications such as photoelectrochemical microelectrode monitoring, antibiotic sensing, temperature sensing, *etc.*[101–103] A photoelectrochemical phenol sensor was fabricated using direct ink writing strategy.[102] Photoelectrochemical microelectrode monitoring is of great importance as a trustworthy strategy over the traditional techniques owing to the advantages this approach provides including high sensitivity, ease of processing, fast response, low background signals, *etc.* In order to meet the demands, a wide variety of photocatalytic agents have been used and integrated with conductive materials to yield photoactive electrodes.[104–106] However, they mainly suffer from weak light absorption and limited trapping of analytes, both of which prevent the practical application of these sensing agents.[107] The fabricated phenol sensor was composed of titania-Ti_3C_2 as a photocatalyst,

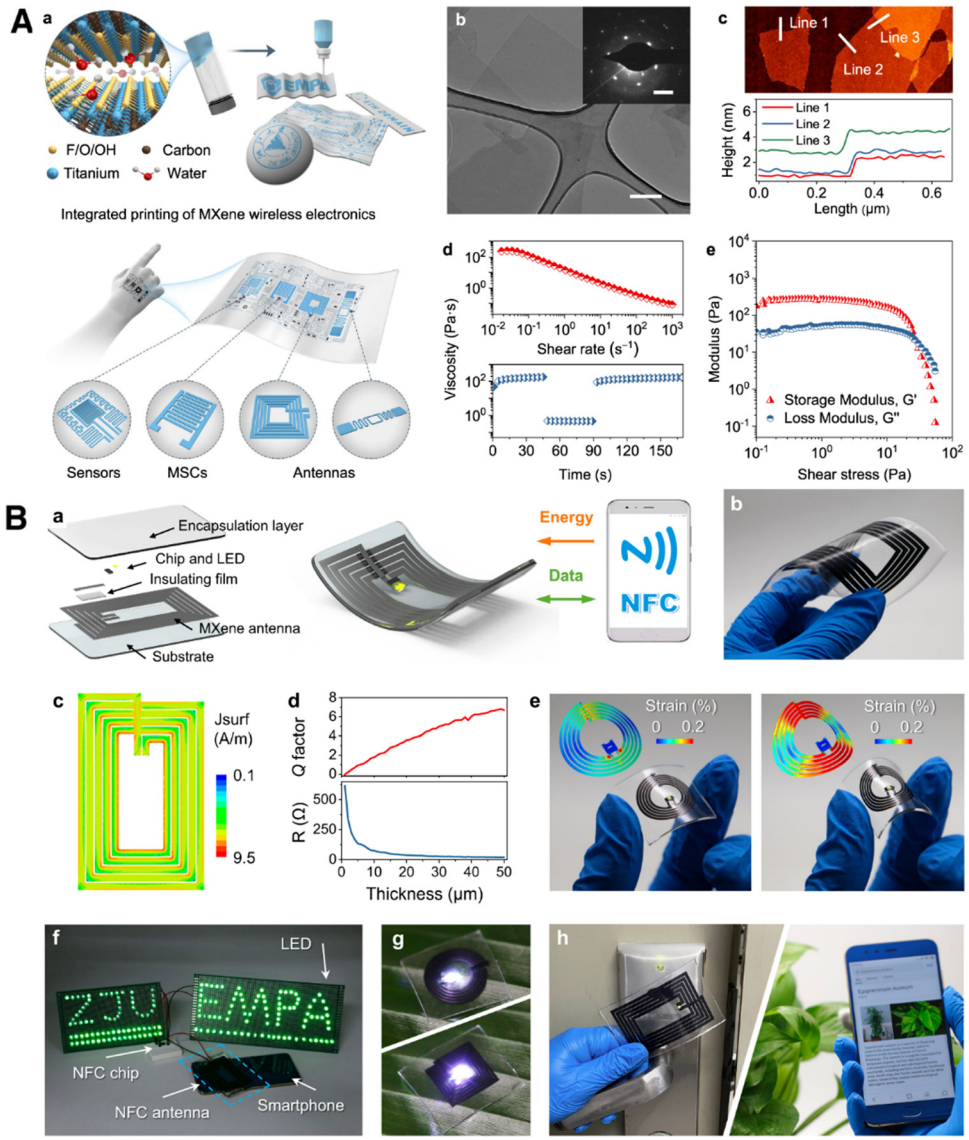

Fig. 4 A flexible wireless electronic sensor based on $Ti_3C_2T_x$ MXene. (A) (a) Schematic illustration of the MXene ink's 3D printing at room temperature; the ink was printed on different substrates to yield flexible wireless electronics like sensors, antennas, *etc.* (b)–(e) Characterization of $Ti_3C_2T_x$ nanosheets by techniques such as TEM and AFM, and rheological properties of the MXene-included ink including storage modulus and loss modulus *vs.* shear stress. Applications of the MXene-included tags as various devices. (B) (a) Fabrication of 3D printed tags and how they communicate with smartphones wirelessly. (b) Photograph of forming MXene ink on polydimethylsiloxane. (c) Distribution of surface current on the tag at 13.56 MHz. (d) Checking the *Q* factor and resistance of the tag for various thicknesses. (e) Photographs taken from the curved tags to check the distribution of strain under bending. (f) The photograph shows that the transmission of electrical energy to the tag from a tag-enabled smartphone could lighten 168 parallel LED lights. (g) Two tags with different shapes with the lighted LEDs. (h) Other applications of the tags like access card for electronic doors (left) and an electronic label to give information about a plant (right). Abbreviation: NFC, near-field communication. Reproduced from ref. 100 under the terms of the Creative Commons CC BY license. Copyright 2022, Nature.

graphene, and molecularly imprinted polyaniline. In here, the ink was composed of a concentrated aqueous solution of graphene oxide/MXene that was printed and lyophilized to fabricate a stable GOM aerogel without any deformation and annealed at a high temperature to produce TiO_2–Ti_3C_2. The viscosity of the fabricated ink showed long-term stability which was increased by reducing the shear rate. Moreover, the rheological analysis confirmed the uniformity of the ink with continuous flow through the needle without blockages during the printing process. The 3D printed structure was found with well-interconnected hierarchical pores in which graphene oxide and titania-Ti_3C_2 had been homogeneously distributed and polyaniline was anchored uniformly as a thin layer on the fibers. This design could not only facilitate the absorption of light, but also provide special binding sites for fast analyte trapping. In the case of phenol detection, the sensor turned out to respond fast with a detection limit as low as 0.4 μM with excellent selectivity and sensing stability.[102] Different types of

antibiotics are being administered to prevent or fight infection, but applying the appropriate dosage of an antibiotic followed by control over the release rate is of great importance because over-dose can induce toxicity and resistance in the pathogens.[108] To monitor antibiotic drug release, a 3D-printed scaffold composed of conductive acrylate-based polymer microlattices was developed on which MXene nanosheets were deposited. Following printing of the polymeric substrate, it underwent dip coating in the MXene ink. Owing to the microporous lattice structure, an effective ion intercalation with improved diffusivity was achieved. The higher surface area of the 3D printed scaffold in this study compared to similar ones with less surface area could provide more electrochemically active sensing surface resulting in the improved detection of gentamicin (1–10 mM) and vancomycin (1–100 mM). Nevertheless, the applicability of the scaffold was assessed towards bone tissue engineering and osteoblast-like MG63; the cells had been seeded on the scaffold to determine the cell compatibility. The results were promising and this scaffold was found to integrate electrical biosensing functions with an implantable scaffold/implant to take better control of drug release.[103] MXene-bonded hydrogels consisting of polyurethane and polyvinyl alcohol with strain and temperature sensing potential were developed through direct ink writing (Fig. 5). Two variables including MXene and glycerol content were optimized to check if there was any effect on the mechanical strength. First, the MXene flakes were homogeneously dispersed in the absence of glycerol and the polymers. Polyurethane and polyvinyl alcohol were then added to the black blend of flakes and heated up to 90 °C in the presence of argon to prevent oxidation of flakes at that temperature. The obtained liquid precursor was transferred into a syringe and printed through a direct ink-writing printer. It is worth mentioning that the ink had undergone a pre-treating process by which de-bubbling took place and the viscous precursor was continuously extruded through the needle driven by air pump pressure and formed on a polyethylene terephthalate substrate. In terms of strain and temperature sensing, the hydrogel was tested and it showed significant strain responses with a gauge factor of 5.7 within 191% strain and the response time was 240 s, and it could tolerate about 5000 cycles. These features endowed the hydrogel with superelastic behavior capable of undergoing large, reversible deformation and recovering its original shape without permanent deformation. Speaking of temperature sensing, the hydrogel exhibited excellent temperature sensitivity with temperature coefficient of resistance of $-5.27\%\ ^{\circ}C^{-1}$ (0–30 °C) and $-0.84\%\ ^{\circ}C^{-1}$ (40–80 °C).[101]

MXene-incorporated 3D- and 4D-printed platforms represent a cutting-edge frontier in the development of smart sensors. These platforms harness the unique properties of MXenes including tunable surface chemistry, high electrical conductivity, and excellent mechanical properties, combined with the flexibility and customization of 3D and 4D printing technologies. These sensors are known to have improved sensitivity and responsivity mainly owing to the excellent electrical conductivity of MXenes, which led to the creation of highly sensitive biosensors. The integration of MXenes with 3D-printed structures provides an opportunity to create sensors with a high degree of responsiveness to environmental stimuli. Another interesting ability of MXene-based 3D-printed sensors

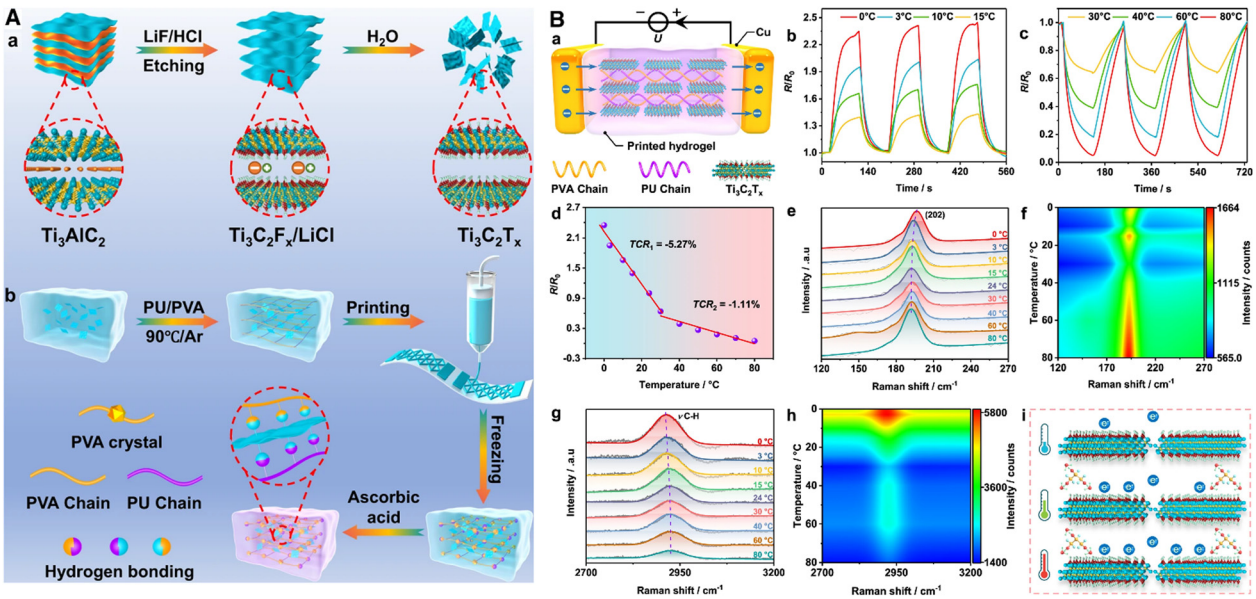

Fig. 5 MXenes hybrid hydrogel with superelasticity and temperature sensing. (A) (a) Step-by-step preparation of $Ti_3C_2T_x$ flakes. (b) 3D printing process of the MXenes and the hydrogel (polyurethane and polyvinyl alcohol). (B) (a) Schematic illustration of temperature sensing related to the printed hydrogel. (b) and (c) Variation in resistance after exposure to different temperatures (starting point was at 24 °C). (d) Temperature coefficient of resistance related to the printed hydrogel. Raman spectra relevant to temperature of (e) and (f) $Ti_3C_2T_x$, and (g) and (h) the printed hydrogel. (i) The mechanism of action by which the hydrogel works as a temperature sensor. Reproduced from ref. 101 under the terms of the Creative Commons CC BY license. Copyright 2022, Nature.

is their detection capability for gases, temperature changes, and also humidity with high precision. These features stem from MXenes' tunable surface chemistry which allows for the detection of different analytes. Speaking of wearable sensors, they are being used increasingly due to their flexibility and lightweight nature; they can monitor physiological signals like motion, heartbeat, respiration, *etc.*, and provide real-time data which is of great importance for healthcare applications.

3.2. Energy storage devices

Recently, there has been a high demand for flexible, wearable, and portable devices, which led to the design and development of powering systems including solar cells, fuel cells, *etc.*[109] The designed systems for flexible power management are of particular interest because the new energy storage ways are indispensable to achieve sustainable energy management. There is no doubt that energy storage will be more and more important in future and so fabrication of active new materials for high-capacity electrodes is essential.[110,111] In the last decade, 2D nanomaterials have opened new opportunities in the field of supercapacitors. Two specific features of these materials are high ion-capacity and fast ion-diffusion attributing to their high surface area and unique electrical properties.[112] Within the 2D family, MXenes exhibit wider chemical varieties than their counterparts with the possibility to tune the surface chemistry, and also, they are endowed with unique reaction spaces making them excellent candidates for energy storage applications.[81]

Lithium-ion capacitors and lithium-ion batteries represent adaptable and cost-efficient power solutions for flexible printed electronic systems, boasting extended lifespans and impressive energy densities.[113] The key requisites for their anode and cathode materials include reduced self-discharge rates and high capacities, which significantly influence lithium-ion batteries' performance.[114] The exploration of recyclable lithium-ion batteries as advanced next-generation power sources is underway due to their specific capacity and safety features. Various designs of flexible lithium-ion batteries have already been developed using lithium-ion battery electrodes successfully fabricated by 3D printing techniques.[115] Although graphite currently dominates the market with respect to lithium-ion batteries' anode material due to great advantages including high stability, low lithium potential, high capacity, and affordability, it has been revealed through theoretical and experimental investigations that Ti_3C_2 MXene shows promise as an alternative anode material.[116] The structural and electronic stability of Ti_3C_2 monolayers and other derivatives of this material—fluorinated and hydroxylated—were elucidated through computational studies (density functional theory) and it turned out that based on the surface modification, this material has potential to behave as a magnetic metal and a semiconductor with a small band gap.[117] Earlier research[117] suggests that pure Ti_3C_2 MXene exhibits some excellent properties such as high lithium storage capacity, low diffusion barriers, and a small operating voltage, making it an appropriate candidate for replacing TiO_2 polymorphs, which are available commercially, in the field of lithium-ion batteries.[118] However, caution is advised against the synthesis of hydroxylated or fluorinated derivatives, as these may impede lithium diffusion and consequently reduce energy storage capacity. Theoretical investigations demonstrating lower ion diffusion barriers in MXene materials align with the outstanding performance observed in experimental studies.[117,119]

There has been an increasing attention towards lithium ion capacitors, which combine a lithium-ion battery anode with a supercapacitor cathode along with an appropriate electrolyte.[120] The design of these capacitors is in such a way that they provide high energy density while maintaining high power density. To achieve advanced electrochemical charge storage, it is necessary for the hybrid lithium-ion capacitor devices to have anodes with greater capacity for reversible lithium-ion intercalation. However, their practical application is hindered by low life cycle and limited rate capability. In this context, MXenes have emerged as promising candidates for lithium-ion capacitor applications due to their remarkable properties. Ultra-thin structure and an open layer in various MXene materials—Nb_2CT_x, Ti_2CT_x, $Ti_3C_2T_x$, and V_2CT_x—facilitate the swift deintercalation/intercalation kinetics of lithium ions. Consequently, MXene materials exhibit characteristics resembling capacitors rather than traditional batteries.[121,122]

Integration of self-powered systems with storage devices has significant effects on the future of energy storage and this necessitates forming various devices directly on a substrate.[123] This research line has led to considerable development in "on-chip" batteries and supercapacitors. In the case of miniaturized electronics, on-chip supercapacitors are considered as appropriate candidates for integration with those electronics; on-chip supercapacitors are ascribed to micro-supercapacitors, which are reputable as high-power devices with high energy density.[124] Using a water-based and viscoelastic MXene ink, 3D micro supercapacitors were fabricated. The extrusion printing technique was adopted to directly form the MXene ink on various substrates including papers and flexible polymer film. The number of deposit layers was carefully controlled to form active materials and electrodes with suitable height. The electrochemical performance of the micro supercapacitor was excellent and the energy density (51.7 μW h cm^{-2}) and areal capacitance (1035 mF cm^{-2} at 2 mV s^{-1}) were exceptional.[88] Free-standing 3D architectures were designed through the extrusion-based 3D printing technique as a multiscale and multidimensional device for different applications including energy storage, catalysis, *etc.* First of all, an additive-free water-based ink consisting of $Ti_3C_2T_x$ flakes was prepared which was a solid-like network with appropriate rheological properties for layer-by-layer 3D printing. The optimized ink was chosen to yield 3D micro supercapacitors with the MXene flakes interdigital fingers. The 3D-printed devices showed an areal capacitance of 2.1 F cm^{-2} at 1.7 mA cm^{-2} and the energy and power density were 0.0244 mW h cm^{-2} and 0.64 mW cm^{-2}, respectively.[70] Somewhere else, a MXene ink was developed which was endowed with high sensitivity and conductivity; from the rheological point of view, the ink for capacitive and battery-type applications was

outstanding enough to yield micro supercapacitors and lithium-ion micro-batteries *via* screen printing on different substrates—wood, fabric, A4 paper, silica-coated stainless steel, *etc.* Referring to the performance of the MXene-based micro supercapacitors, the areal capacitance and energy density were 1.1 F cm^{-2} and 13.8 μW h cm^{-2}, respectively. The MXene supercapacitor exhibited excellent flexibility and 60 V output in series, whereas the MXene-based lithium-ion micro-batteries showed outstanding areal energy density (154 μW h cm^{-2}). Without using any external power source the platform was able to monitor deformation with a fast response (35 ms) precisely and repeatedly.[89] Having all the merits of the 3D printing technique, 4D printing is affected by the fourth dimension of time and different properties like functionality, property, and shape can be changed over time upon exposure to external stimuli (*e.g.* light, pH, heat, *etc.*).[125] To achieve a scalable production, an advanced 4D printing technique has been developed to yield MXene hydrogels using a polymeric crosslinker—poly(3,4-ethylenedioxythiophene):poly-(styrene sulfonate) (PEDOT:PSS). Unlike the conventional 3D printing method which yields dissolvable MXene sol patterns, this study reported on the 4D printing approach which involved the creation of cross-linked MXene hydrogels with improved mechanical properties through a straightforward self-assembly process when exposed to heat. Dimethyl sulfoxide and H_2SO_4 as the additives were found to facilitate the self-assembly; since the shape of hydrogels was dependent on the heat (90 °C), various shapes including cylinders, fibers, cones, and hemispheres were developed using different molds. Once PEDOT and PSS are added, they tend to form a core–shell structure; PEDOT with a hydrophobic nature and a positive surface charge formed the core, while the hydrophilic PSS with a negative surface charge formed the shell making the core–shell structure dispersible in water. The addition of MXenes led to the formation of electrostatic and hydrogen bonding between PEDOT and PSS. The negatively charged MXene flakes attached to $PEDOT^+$ chains and these chains underwent oxidation from benzene to quinoid configurations. The addition of H_2SO_4 was synchronized with the protonation of PSS^- and weakening of the electrostatic bonding between PEDOT and PSS which led to the formation of more coiled $PEDOT^+$ with a linear structure and elongated conjugation lengths, whereas more PSS^- chains were dissolved in the acidic medium. Those PEDOT chains interacted with themselves and MXenes, through physical and electrostatic interactions, respectively, and shaped the 3D networks. DMSO with polar nature promoted the removal of PSS^- similar to H_2SO_4 and synergistically facilitated the self-assembly process. This method is an applicable strategy towards preparation of various hydrogels consisting of MXenes—$Ti_3C_2T_x$, Nb_2CT_x, and $Mo_2Ti_2C_3T_x$. It is worth mentioning that the MXenes adopted in this study have different atomic layers and transition metals with distinct structures and characteristics. Moreover, the composite hydrogels' geometries can be precisely customized to produce intricate architectures such as rectangular hollow prisms, micro lattices, and micro supercapacitor units. Despite their varied designs, these hydrogels exhibit excellent wettability, high surface areas, and high electrical conductivity. The hydrogel electrodes incorporating $Ti_3C_2T_x$ display significant areal capacitance (3.32 F cm^{-2} at 10 mV s^{-1}), ultrahigh specific capacitance (232.9 F g^{-1} at 10 V s^{-1}), and rate capabilities independent of mass loading and thickness. The performance of 4D-printed hydrogel micro supercapacitors was assessed at −20 °C and the capacitance retention was 82.2%, while this value was 90.6% at 0 °C. The power and energy densities of micro supercapacitors were 6.96 mW cm^{-2} and 92.88 μW h cm^{-2}, respectively, indicating the promising potential of these platforms as efficient storage devices (Fig. 6).[76]

Light-driven soft robotics have drawn considerable attention in recent years for solar energy harvesting devices; liquid crystal elastomer actuators, which are known to be triggered by photothermal nanofillers, have been applied extensively for developing light-driven soft robots.[126,127] A wide variety of nanofillers have been adopted for fabricating photosensitive liquid crystal elastomers among which graphene oxide, carbon nanotubes, gold nanoparticles, MXenes, *etc.* could be mentioned. Throughout the actuation process, the exposure of incorporated nanofillers to visible/NIR light is synchronized with the absorption of light, turning it into heat, and so increasing the local temperature; the generated heat has an effect on the structure of the liquid-driven elastomer and makes the aligned mesogens disordered, which leads to a shape change. Once the light irradiation goes off, the elastomer regains its original shape again.[128–130] One of the main disadvantages revolving around photosensitive agent-incorporated light-driven elastomers is the shear stress at the interface of nanofillers and the elastomer's matrix; this is caused by inhomogeneous thermal conduction, resulting from the incompatible elastic modulus of the nanofiller and the elastomer. This incompatibility leads to weak stress transfer and interfacial slipping gaps and leaves negative effects on different properties—mechanical, cyclic stability, and actuation capability.[131,132] A versatile strategy was reported in a recent study to prevent the poor physical interactions between the elastomer molecules and the nanofiller; the authors succeeded in forming a chemical bonding between two phases to inhibit nano-interfacial slipping gap. Different nanofillers have been added to the elastomer including copper nanoparticles, copper sulfide nanowires, and $T_3C_2T_x$ nanosheets. The abundant functional groups on the surface $T_3C_2T_x$ nanosheets allowed easy functionalization through silanization reaction. The amine end group on the surface of nanosheets was able to form covalent bonds with the liquid crystal monomer matrix *via* the aza-Michael reaction. As indicated, 4D printing was adopted to align the liquid crystal elastomer to form complex multi-dimensional shapes. Using a polarized microscope, the orientation of materials through the 4D printing process was checked when irradiation condition had been applied. After rotating the sample by 45°, changes in the brightness and darkness of images were observed indicating the effective orientation of liquid crystal elastomer actuators through the printing process. Moreover, the tubular actuators were fabricated around a cylindrical axis. Upon applying NIR light, the surface temperature increases and causes the tubular actuator to contract and bend towards the light source. In this study, different structures were fabricated to show

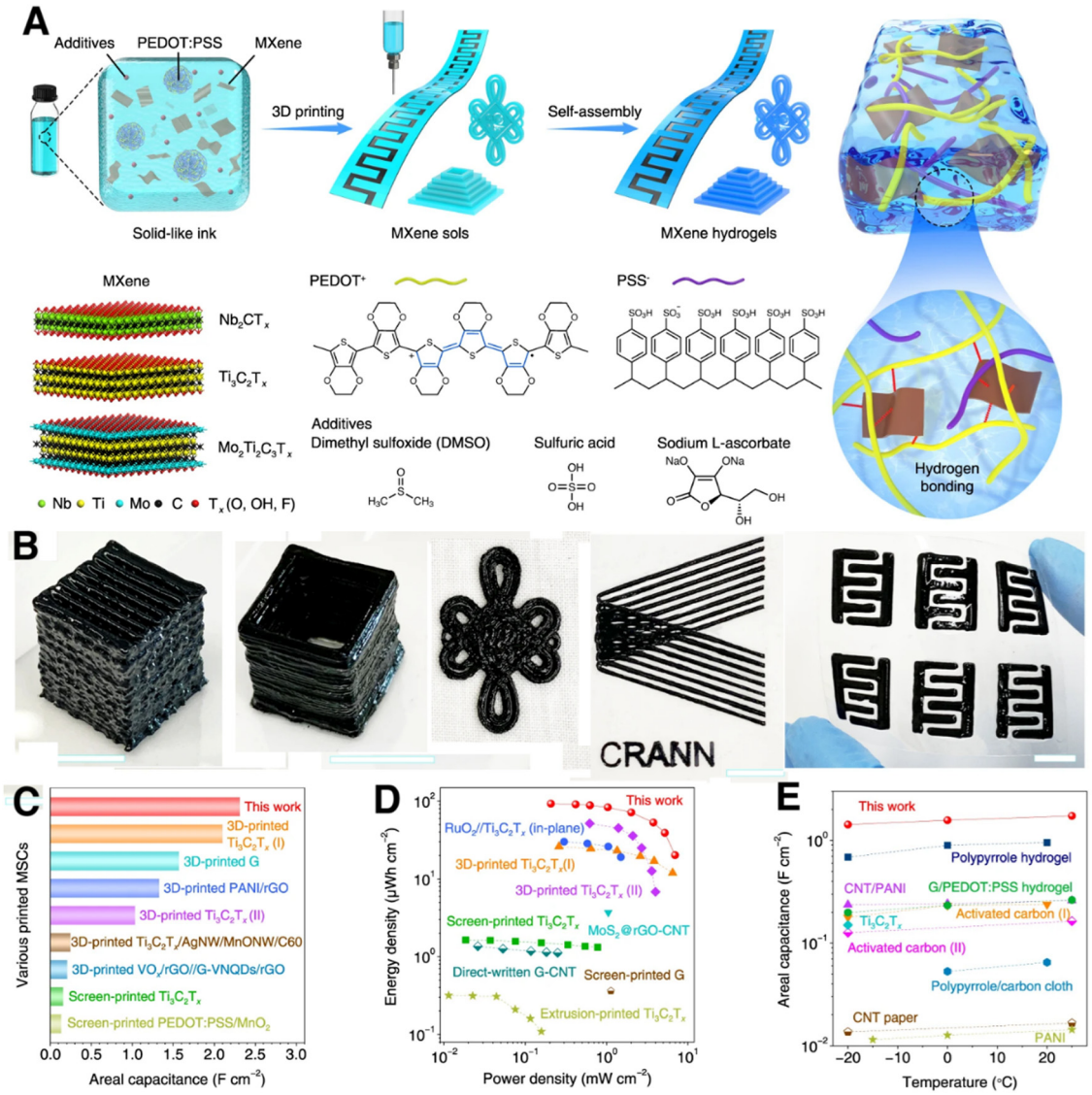

Fig. 6 4D-printed composite hydrogels incorporating different MXenes for energy storage applications. (A) Schematic illustration of the hydrogels' preparation process; the combination of PEDOT:PSS, MXenes, and other additives including DMSO, H_2SO_4, and sodium L-ascorbate led to the formation of printable ink followed by fabrication of designed patterns, and subsequently a self-assembly process. (B) The photographs taken from different designed patterns printed from the composite hydrogels, from left to right, include $Ti_3C_2T_x$ hydrogels (micro lattice and rectangular) on a glass slide, a Chinese knot and the logo (CRANN) made of Nb_2CT_x hydrogels, and flexible micro supercapacitors on PET film composed of the hydrogel incorporating $Mo_2Ti_2C_3T_x$. The heat-induced self-assembly led to the formation of hydrogels with different shapes. (C) Making a comparison of the value of areal capacitance of the composite hydrogel micro supercapacitors made of $Ti_3C_2T_x$ reported by Gogotsi *et al.*[76] with other micro supercapacitors yielded through 3D printing. (D) Ragone plots related to the composite hydrogel ($Ti_3C_2T_x$) developed in the study by Gogotsi *et al.*[76] and various high-performance micro supercapacitors. (E) Comparison of the areal capacitance of 4D-printed hydrogels with that of others upon exposure to temperature. Abbreviations: PEDOT, poly(3,4-ethylenedioxythiophene); PSS, poly(styrene sulfonate). Reproduced from ref. 76 under the terms of the Creative Commons CC BY license. Copyright 2022, Nature.

the versatility of liquid crystal elastomer's applications and in this regard, a solar panel was fixed on the upper side of tubular actuator to design a smart solar energy harvesting device. This device was found to actively track and bend towards the light source. Upon applying 1 W cm^{-2} incandescent light, the rotation angle reached 13°. The open-circuit voltage and cyclic irradiation experiments revealed that this device was effective enough to boost solar energy utilization and maintained stability under prolonged cyclic actuation conditions.[133]

MXene-incorporated 3D- and 4D-printed platforms hold significant potential in the field of energy storage, specifically for developing advanced batteries, supercapacitors, and other energy storage devices. These platforms integrate the physicochemical properties of MXenes, such as electrical, electrochemical, and mechanical properties, with the design flexibility and customization of 3D and 4D printing technologies. This combination leads to the development of energy storage devices with improved electrochemical performance due to the

high surface area and conductivity of MXenes and customized electrode architecture (through 3D-printing, highly porous structures can be designed which maximizes the interaction of MXenes with the electrolyte). These devices are endowed with structural integrity and mechanical flexibility; 3D-printing technologies can yield MXene-based structures mechanically robust and flexible making them suitable candidates for wearable energy storage devices. Noteworthily, these structures can preserve their performance even under mechanical deformation. Moreover, they have a high loading capacity; the loading of MXenes in the 3D-printed scaffolds leads to the structural integrity of the electrodes and so greater energy storage capacity per unit volume or weight.

3.3. Biomedical applications

Additive manufacturing has revolutionized biomedicine with its capability to design complex structures with high precision. This technique and all other technique derived from it are able to create personalized biomedical devices and implants suitable for each individual's anatomy, which leads to an improvement in the functionality.[134] One of the most important features of additive manufacturing is the creation of intricate structures such as 3D scaffolds and implants for disease therapy and tissue regeneration; these structures can be designed in such a way that they mimic the natural environment of cells promoting better integration and regeneration.[135,136] MXenes hold great promise in biomedicine due to many advantageous features they possess such as high surface area and unique surface chemistry, which makes them suitable for drug delivery, strong optical properties making them promising candidates for biomedical imaging and light-sensitive therapeutic approaches, electrical conductivity, antimicrobial activity, *etc.*[83,84,137] In this section, some of the most important fields that have adopted additive manufactured MXenes are covered including cancer therapy, drug delivery, antibacterial activity, and tissue regeneration.

Throughout orthopedic surgery, it is common to take advantage of random skin flaps for repairing the tissue defects caused by trauma, tumor, congenital deformities, *etc.* However, insufficient blood supply to the skin flaps causes necrosis especially when the length-to-width ratio is high. Different approaches have been taken into consideration to address this issue such as administration of vascular endothelial growth factor locally and various therapeutic drugs (*e.g.* vasodilators, sympathetic blocking drugs, *etc.*), but they suffer from some disadvantages—short half-life, side-effects attributed to the administration of high dosages, and tumorigenic risks.[138,139] To promote vascularization and address the skin flap regeneration, MXene-incorporated hollow fibrous scaffolds were designed through a microfluidic printing strategy (Fig. 7(A)–(D)). Firstly, all compounds including MXene nanosheets (Ti_3C_2), alginate, and *N*-isopropylacrylamide were polymerized in the microfluidic coaxial channels and then the bio-ink was used for the creation of scaffolds. There was a correlation between *N*-isopropylacrylamide and the MXenes, which was the thermosensitivity of the polymer and the photothermal conversion capacity of the nanosheets. Upon applying the NIR irradiation, the nanosheets would increase the temperature due to the photothermal conversion making control over shrinkage and swelling behaviors of the polymer; this effect could facilitate enrichment of cells within the scaffold's structure. It is noteworthy that vascular endothelial growth factor was also loaded in the scaffold, which upon applying NIR was released and promoted the migration and proliferation rate of human umbilical vein endothelial cells. *In vivo* studies revealed that the 3D-printed scaffolds, which were stimulated with NIR, enhanced skin flap survival by stimulating angiogenesis and reducing inflammation and apoptosis in this tissue.[90] Skin as the largest organ in the human body is the first barrier to any external potential danger, and injury in this organ means loss of function at the site and so there is a high probability for infection and even death.[140] In this regard, a wide variety of wound dressings have been designed so far and applied, but more attention has been paid recently to more advanced and multifunctional ones.[141,142] One of those advanced wound dressings is microneedle-based patches because besides having the basic requirements of a wound dressing such as biocompatibility, mechanical properties, exudate absorption, *etc.*, they are capable of releasing biological moieties more effectively in the wound's area.[143] A versatile extrusion-based 3D printing strategy has been adopted to fabricate a spidroin-incorporated microneedle patch in combination with MXene nanosheets as a self-healing and photo-responsive platform for wound healing applications. The production process of this platform is shown in Fig. 7(E), where the scaffold is found to consist of a top scaffold and cactus-inspired microneedles; the ink by which the platform had been developed was composed of polyurethane, *Aloevera* gel, and spidroin doped with MXenes. The ratio of these three compounds was adjusted so that the produced ink showed good viscosity and ideal rheological features that provided continuous printing. MXenes along with spidroins led to great biocompatibility, motion monitoring, and photothermal effect. The polyurethane and spidroins gave great mechanical properties to the dressing and the high electrical conductivity of MXenes also helped the platform to sense and monitor the wound status. On the other side, upon NIR irradiation, the increase in the temperature due to the excellent photothermal conversion of MXenes improved the drug release in the wound's bed. The biological assessments are indicated through Fig. 7(F)–(I), where both *in vitro* and *in vivo* studies are indicated; the cells are attached on the microneedle scaffolds up to 5 days and the proliferation rate has experienced a constant increase over time showing the cell compatibility of scaffolds. Speaking of *in vivo* experiments, these treatments on the animal model were performed for up to 9 days and different samples were applied and it is clear that only the sample stimulated with NIR could enclose the wound after 7 days, while the rest failed to do so in the same time interval. As explained earlier, the photothermal effect improved the drug release and thereby significantly enhanced the healing rate.[144]

One of the main issues that is normally overlooked in bone-related therapy and regeneration is the soft tissue damage

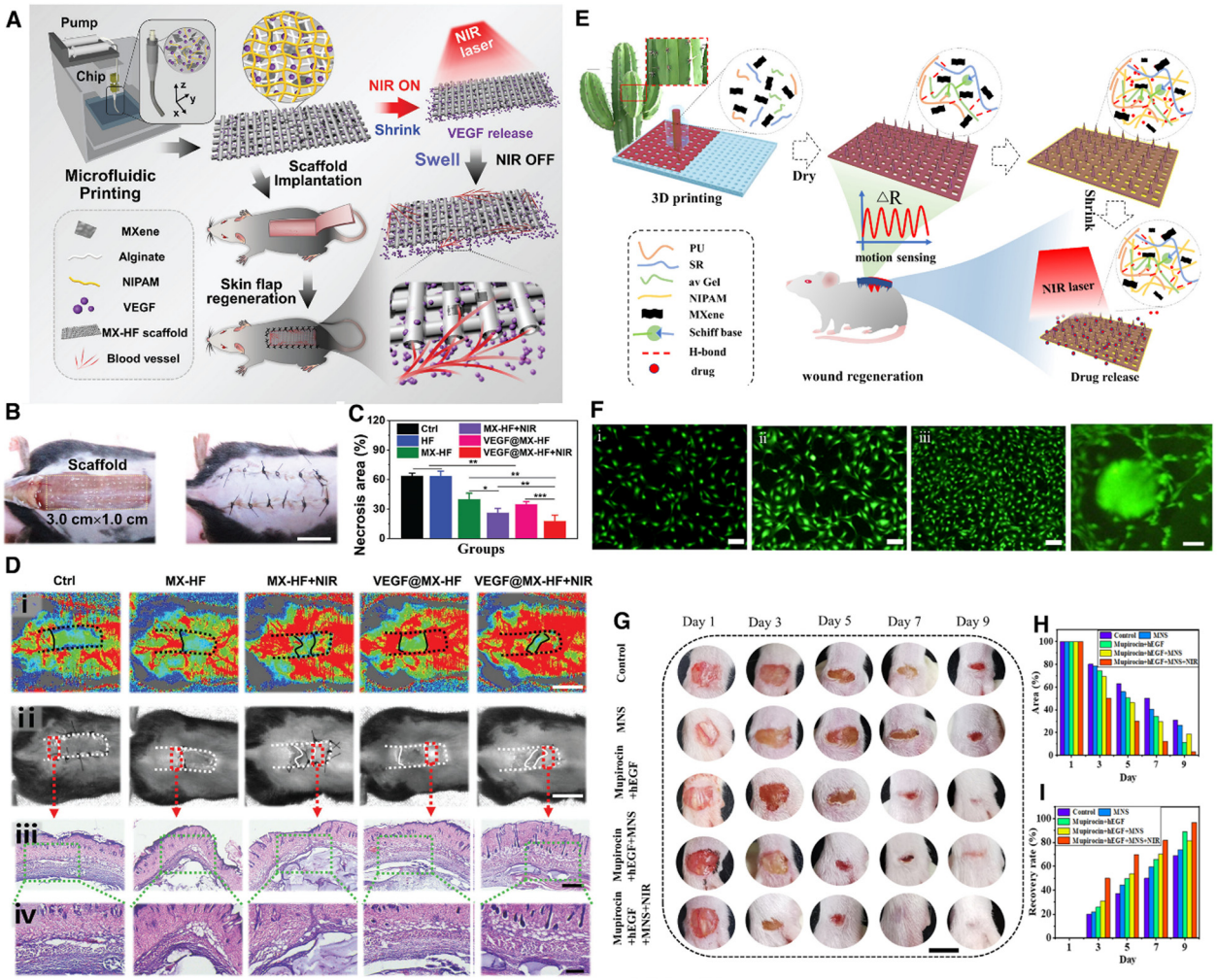

Fig. 7 3D-printed composite structures incorporating different MXenes for soft tissue regeneration. (A) Schematic illustration of fabrication of the MXene-incorporated alginate-NIPAM through microfluidic 3D-printing for skin flap regeneration; the photothermal conversion of MXene nanosheets allowed shrinkage–swelling in the structure of thermo-responsive NIPAM and this effect facilitated the infiltration of cells and tissue in the scaffolds' channels. (B) Applying the skin flap in an animal model followed by implanting the scaffold on the defect and subsequently suturing the flap. (C) The necrosis area related to flaps treated with different samples after 9 days (*$P < 0.05$, **$P < 0.01$, and ***$P < 0.001$). (D) Performing histological analysis of the skin flaps treated with different samples: (i) blood flow images, (ii) photos of skin flaps, and (iii) and (iv) Hematoxylin and eosin (H&E) staining of the necrosis area and survival area ascribed to the skin flaps treated with various scaffolds. Abbreviations: MX-HF, MXene-incorporated hollow fibrous; VEGF vascular endothelial growth factor; NIPAM, *N*-isopropylacrylamide. Reproduced from ref. 90 under the terms of the Creative Commons CC BY license. Copyright 2022, Wiley. (E) Schematic illustration of the fabrication process and application of the MXene-incorporated microneedle patch. (F) Fluorescence images related to the 3T3 cells on the microneedle patch after 1, 3, and 5 days in a row from left to right (scale bar: 100 μm) and the image on the right side is related to 3T3 cells adhering on the MXene-incorporated microneedle patch after 5 days (scale bar: 50 μm). (G) Treatment process of different wounds applied on the forelegs of mice (scale bar: 500 mm). Quantification of (H) the wound area (%) and (I) recovery rate (%) up to 9 days of treatment with different samples *in vivo*. Abbreviations: PU, polyurethane; SR, spidroin; av gel, *A. vera* gel; NIPAM, *N*-isopropylacrylamide; MNS, microneedle scaffold; hEGF, human epidermal growth factor. Reproduced with permission from ref. 144. Copyright 2022, American Chemical Society.

surrounding the bone defects,[145,146] which is a challenging issue because promoting soft and hard tissues at the same time requires the combination of different bioactive agents/biomaterials or taking advantage of multifunctional biomaterials capable of inducing both. For instance, bioactive glass and hydroxyapatite have been considered for both applications as bioceramics and collagen as a biopolymer has been applied in soft and hard tissue regeneration.[147–150] The synergistic soft and hard tissue regeneration potential of photoactivated MXene nanosheets was assessed *in vitro* and *in vivo* in different models. The biomaterial was found to promote extracellular signal-regulated kinases' phosphorylation by enhancing the expression levels of heat shock protein 70 (HSP 70) and it led to the acceleration of stem cells differentiation towards osteogenesis. On the other side, the soft tissue regeneration in *in vivo* models indicated the high potential of the nanosheets in promoting epithelial cell migration and angiogenesis.[151] To address the same problem, an interesting recent study had developed 3D-printed scaffolds composed of gelatin methacryloyl, hyaluronic acid methacryloyl, and $Ti_3C_2T_x$

MXene nanoparticles for skeletal muscle tissue regeneration (Fig. 8). The bioink was composed of gelatin methacrylate (GelMA), hyaluronic acid modified methacryloyl (HAMA), and different concentrations of MXene in PBS, and was mixed with C_2C1_2 myoblasts before printing. The bioink was found to be excellent in terms of printability with structural integrity, biocompatibility, and microporous structure. Addition of MXene to this solution improved its mechanical strength, and the combination of these three compounds contributed to its ideal stiffness and elasticity. C_2C1_2 cells were exposed to the scaffolds to assess if they can be differentiated into skeletal muscle cells and the results confirmed the successful differentiation without using any supportive myogenic agents. The up-regulation of early and late myogenic markers was observed through genetic analysis and also the *in vivo* experiments on mice with volumetric muscle loss showed an improvement in muscle regeneration with minimum immune response when the scaffolds had been applied.[152]

Myocardial infarction is an important and dangerous cardiovascular disease in which coronary arteries are blocked and cause ischemia followed by damage to the cardiac tissue.[153] Recently, various conductive biomaterials are applied in cardiac tissue engineering, among which carbon nanotubes, gold, graphene, *etc.* can be mentioned. However, the cytotoxicity concerns revolve around these materials, raising the need for alternatives. MXenes with excellent properties like biocompatibility, high surface area, high electrical conductivity, hydrophilicity, *etc.* are regarded as promising potential materials in this field.[154,155] Tissue engineered cardiac patches with conductive $Ti_3C_2T_x$ MXene were developed through aerosol jet printing for cardiac repair. The MXene nanosheets were printed on the polyethylene glycol hydrogel to come up with electroconductive patches to promote the alignment of cardiomyocytes. The integration of MXene nanoflakes into non-conductive hydrogels was found to improve the synchronous beating of human induced pluripotent stem cell derived cardiomyocytes and the electroconductivity enhanced the electrophysiological coupling of the substrate and the infarcted area.[156]

As a general term, bone cancer refers to osteosarcoma, chondrosarcoma, and fibrosarcoma and this cancer type is divided into two—primary (skeletal system cancer) and secondary (metastasis from primary cancers such as breast, prostate, and lungs).[147,157] Destructive surgery like amputation and/or limb salvage surgery is the main treatment that a patient receives at the first stage because osteosarcoma is a mineralized tumor and excision of this tissue is a challenging task for a medical practitioner. Following surgery, multidrug chemotherapy treatment has been reported to enhance the survival rate of patients significantly.[158–160] It is known that after surgery, there is a high risk of tumor recurrence due to the remaining cancerous cells in the bone defect highlighting the importance of localized cancer therapy.[161,162] Speaking of MXene-based 3D printed structures for bone cancer therapy and regeneration, one of the most useful strategies which has been adopted is dip coating of a ceramic scaffold in the MXene solution for surface modification.[163,164] This approach allows high photothermal conversion of MXene nanosheets on the surface. In this regard, the ink is prepared and the 3D structures are fabricated through additive manufacturing and subsequently, they undergo heat treatment for sintering. Then the scaffolds are soaked in the MXene solution for physical attachment on the surface which normally changes the white color of the pristine scaffold into grey and/or black indicating the successful coating of the nanosheets on the scaffolds (Fig. 9).[165] In here, Ti_3C_2 nanosheets were deposited on the surface of 3D-printed bioactive glass scaffolds for simultaneous bone cancer therapy and regeneration. The idea was to take advantage of photonic hyperthermia to eradicate cancerous cells *via* the MXenes and repair the bone tissue through the bioactive glass scaffolds. The anticancer potency of MXene-coated scaffolds was tested *in vivo* on female BALB/c nude mice bearing SAOS-2 bone tumors. The tumors were grown subcutaneously to reach the size of 120 mm^3 and then the photothermal treatments were performed; NIR laser irradiation (808 nm, 1.0 W cm^{-2}, 10 min) was applied to the tumors in which the scaffolds had been implanted one day after the implantation. It was found that the temperature of tumor was elevated up to 63 °C after just 2 min laser irradiation, whereas the pristine bioactive glass scaffolds did not experience the same trend and the temperature was 37 °C. Terminal deoxynucleotidyl transferase-mediated dUTP-biotin nick end labeling staining and hematoxylin and eosin were used to qualitatively measure the tumor's ablation efficacy of surface-modified scaffolds and both assays unanimously revealed that the number of apoptotic cells after the photothermal ablation by surface-modified scaffolds was competitively higher than the control.[165] One of the main obstacles revolving around photothermal treatment for bone cancer is the limitation of NIR penetration depth. Bone tumors must be removed through surgery, and based on the size of tumor, there would be a defect left behind which requires to be filled. Since photothermal treatment is limited by the penetration depth of NIR, there is one solution recommended by Pan *et al.*;[165] they suggested to apply NIR irradiation just after implantation of the surface-modified scaffold in the defect to avoid light absorbance by soft tissue (*e.g.* the muscular layer, subcutaneous tissue, skin, *etc.*) followed by stitching up the wound. In this regard, the treatment would be similar to exposing a superficial tumor to NIR rather than a deep tumor and so the photothermal therapy (PTT) would achieve excellent therapeutic outcomes.

Infection has long been a potential danger which can result in surgery failure. Following various bone-related surgeries, bone infection by *S. aureus* can cause joint deformity, amputation, and even death.[166,167] To manage the situation, antibiotic therapy is being performed clinically and a wide variety of drugs are administered systemically in high doses; the failure rate of this therapeutic approach is estimated at about 20% and long-term administration of antibiotics increases the risk of bacterial resistance.[168] Therefore, antibiotic-free strategies are of great importance due to these problems. A multifunctional scaffold composed of copper oxide, tricalcium phosphate, and Ti_3C_2 nanosheets with an internal and external sandwich

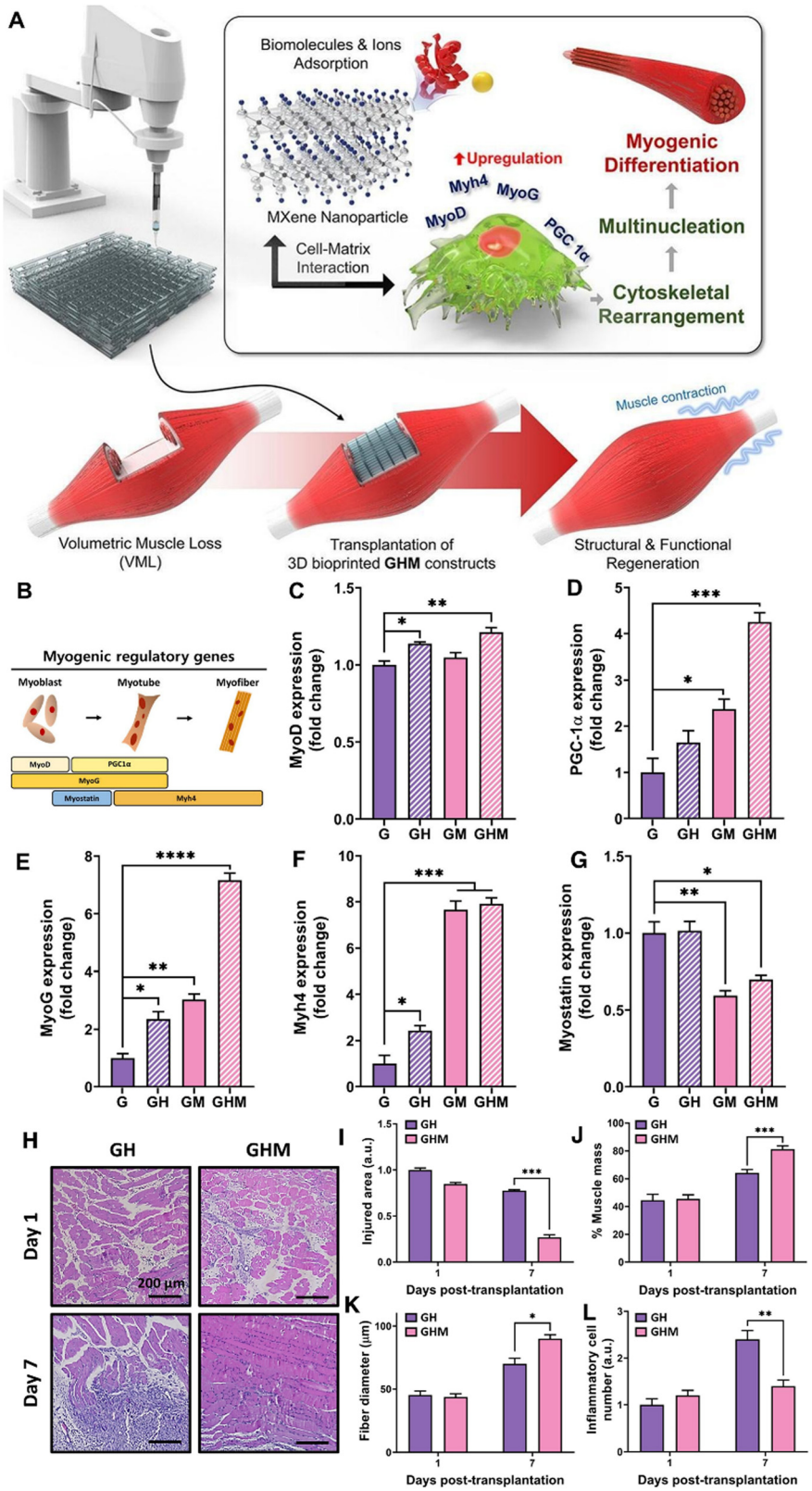

Fig. 8 Skeletal muscle tissue regeneration through MXene-incorporated 3D-printed scaffolds. (A) A schematic illustration of MXene-incorporated gelatin methacryloyl and hyaluronic acid methacryloyl scaffold's preparation and its positive effects towards skeletal muscle regeneration—biocompatibility, structural microporosity and integrity, and myogenic differentiation. (B) Schematic illustration indicating the myogenic regulatory genes. The results related to qRT-PCR of (C) MyoD, (D) PGC-1α, (E) MyoG, (F) Myh4, and (G) myostatin from myoblasts. (H) The images related to the tibialis anterior cross sections stained through H&E staining; the nucleus and cytosol are indicated in purple and pink, respectively. Quantitative results from H&E stained images related to (I) volumetric muscle loss injury area, (J) muscle mass, (K) muscle fiber diameter, and (L) inflammatory cell. Significant difference from the control (*$p < 0.05$, **$p < 0.01$, ***$p < 0.001$, and ****$p < 0.0001$). Abbreviations: VML, volumetric muscle loss; G, gelatin methacryloyl; GH, gelatin methacryloyl-hyaluronic acid methacryloyl; GHM, gelatin methacryloyl-hyaluronic acid methacryloyl-MXene nanosheets. Reproduced with permission from ref. 152. Copyright 2024, Elsevier.

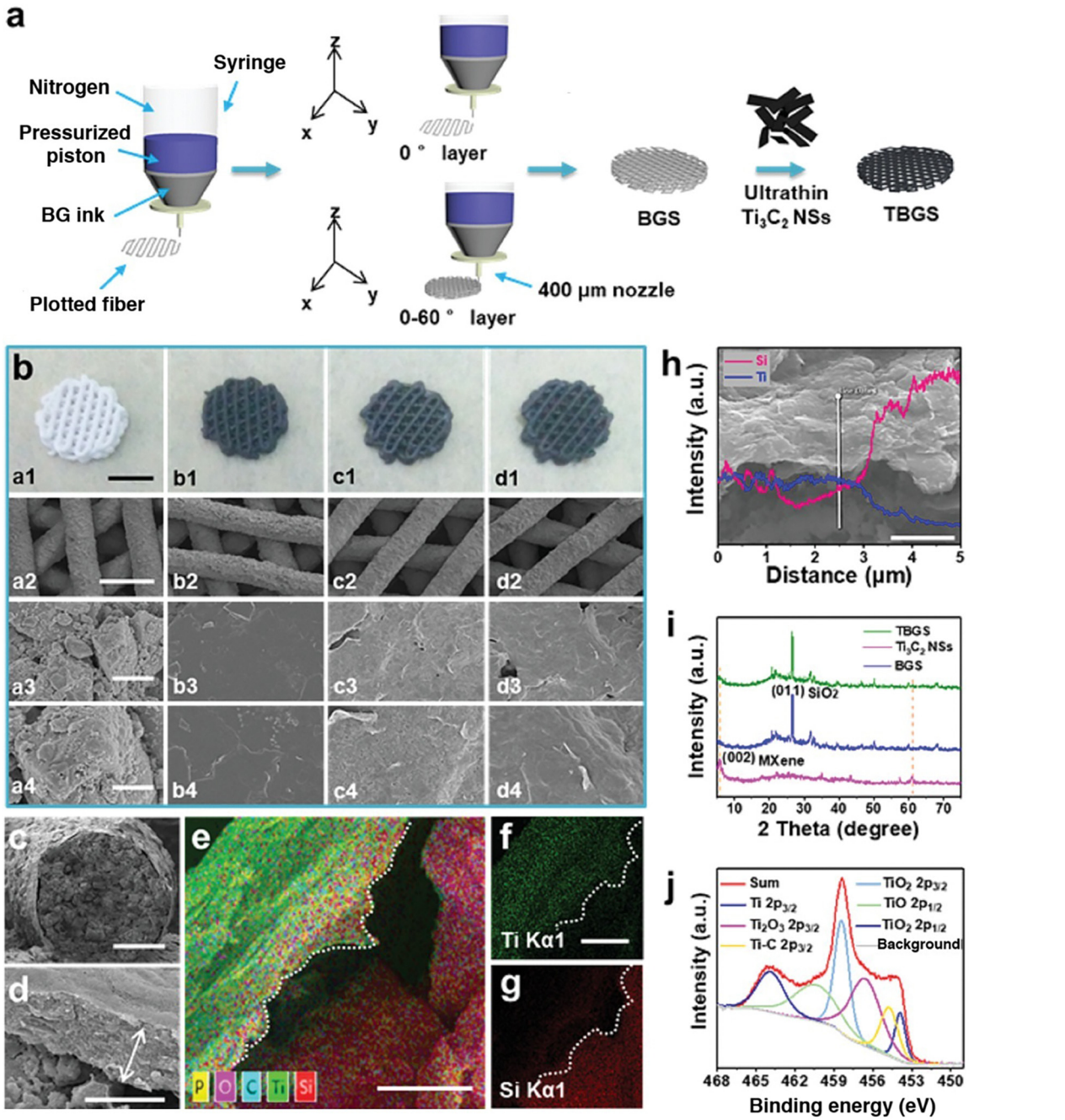

Fig. 9 Surface modification of 3D-printed bioactive glass scaffolds with Ti_3C_2 nanosheets for bone cancer therapy and regeneration. (a) (a1)–(d1) Schematic illustration of bioactive glass scaffolds' preparation followed by surface coating of the nanosheets through the dip coating technique. (b) (a2)–(d4) Digital photographs of the bare bioactive glass scaffold (white) with the nanosheets with different content; SEM micrographs of each sample below the digital photographs exhibiting the topography of the samples before and after surface modification. (c)–(g) Surface topography at higher magnifications along with elemental mapping which proves the successful coating of the nanosheets on the bioactive glass fibers. (h) SEM micrograph of the surface-modified scaffold with EDS analysis (scale bar: 3 μm). (i) XRD patterns of different samples before and after surface modification. (j) XPS spectra related to the surface-modified scaffold. Abbreviations: TBGS, Ti_3C_2-coated bioactive glass scaffold; BGS, bioactive glass scaffold. Reproduced from ref. 165 under the terms of the Creative Commons CC BY license. Copyright 2020, Wiley.

structure was designed and fabricated through the 3D printing technique. The idea was to take advantage of two potential antibiotic-free approaches—release of metal oxide ions and photothermal activity—against bone infection and also stimulate vascularization (Fig. 10(A)). An interesting point in this study is to adopt a programmed temperature control for PTT by which no negative effect would be induced on healthy cells. To do so, a short-term PTT was first applied through irradiating an 808 nm NIR laser to the scaffolds, which triggered the MXenes on the surface to turn the light into heat,

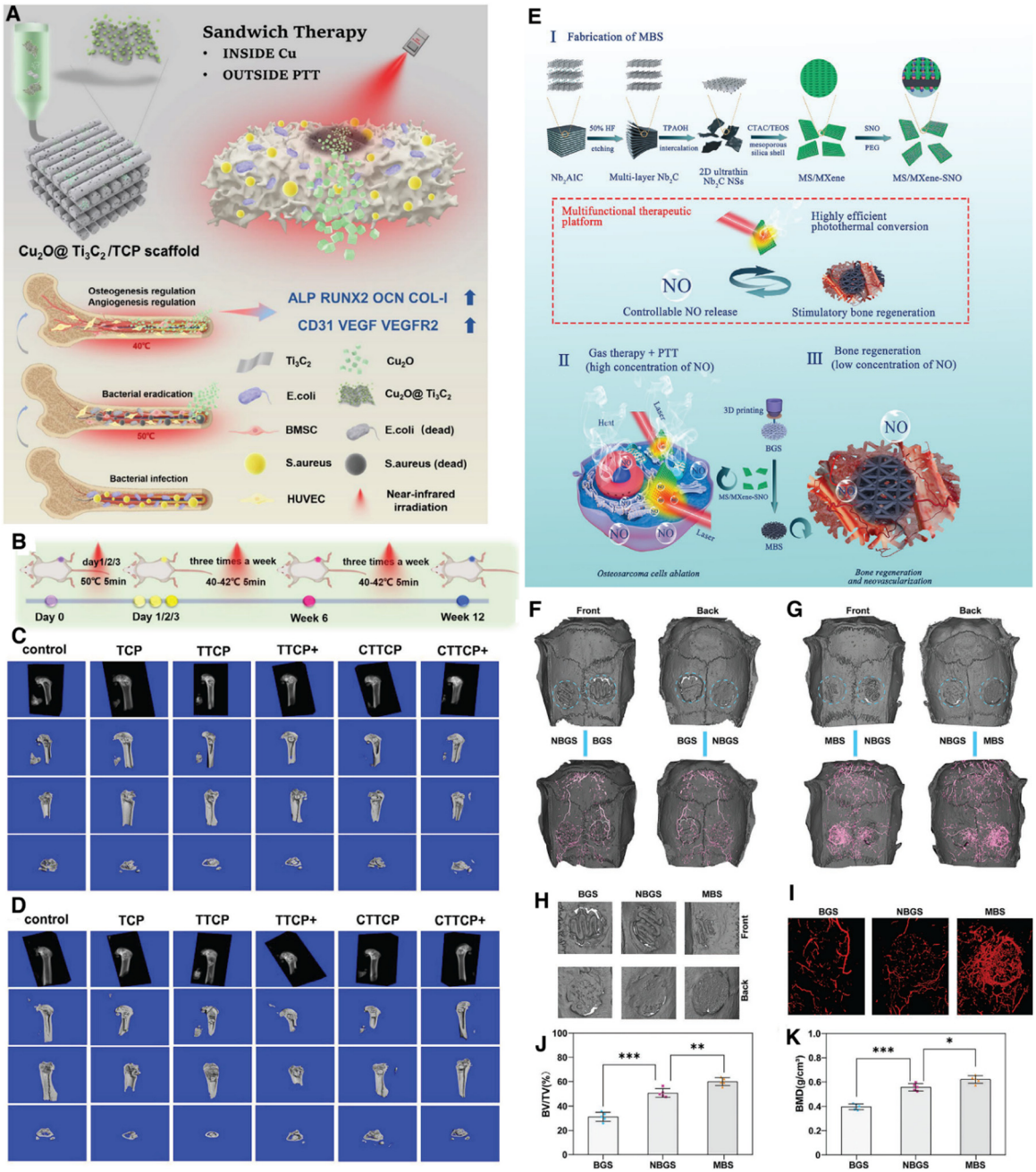

Fig. 10 3D-printed composite structures incorporating different MXenes for disease therapy and hard tissue regeneration. (A) Schematic illustration of a multifunctional scaffold composed of copper oxide, Ti_3C_2 nanosheets, and tri-calcium phosphate for bone infection therapy and regeneration. (B) Bone infection therapy and regeneration in animal models when tested *in vivo* up to 12 weeks. Micro-CT images related to the femur of rats treated with different scaffolds after (C) 6 and (D) 12 weeks (the samples with plus (+) sign were combined with NIR stimulation). Abbreviations: TCP, tri-calcium phosphate; TTCP, Ti_3C_2/TCP; CTTCP, Cu_2O@Ti_3C_2/TCP. Reprinted with permission from ref. 169. Copyright 2023, Wiley. (E) Schematic illustration of the multifunctional Thera generative platform composed of mesoporous silica-coated MXene nanosheets deposited on 3D-printed bioactive glass scaffolds; the combination of PTT and gas therapy resulted in the eradication of cancer cells followed by repair of the damaged bone. (F) and (G) 3D images related to the cranial bone defects and vessel formation treated with different scaffolds after 16 weeks of implantation. (H) and (I) Images of the bone defect area and peripheral blood vessels ascribed to various scaffolds after 16 weeks of implantation. Quantitative results attributed to (J) the bone volume/tissue volume (BV/TV) and (K) bone mineral density (BMD) based on the analysis performed through micro-computed tomography (*$P < 0.05$, **$P < 0.01$, and ***$P < 0.001$). Abbreviations: BGS, bioactive glass scaffold; NBGS, Nb_2C-integrated BGS; MBS, Nb_2C wrapped with *S*-nitrosothiol-grafted mesoporous silica with 3D-printed BGS. Reprinted with permission from ref. 172. Copyright 2020, Wiley.

and this stimulation led to the rapid increase of temperature up to 50 °C, which is strong enough to kill bacteria. Next, a low-periodic photothermal stimulation was applied elevating the temperature up to 40 °C, which has potential to promote

bone tissue growth. On the other side, liberation of copper ions from the inner side of the scaffold over longer time intervals not only improved the antibacterial activity of the scaffolds, but also improved the vascularization. To assess the antibacterial and bone regeneration capabilities of samples, the scaffolds were contaminated with *S. aureus* (10^8 mL^{-1}) and then implanted in the femur of rats. 4 weeks after the implantation, the tissues in the close vicinity of scaffolds were taken for histological analysis; in the case of control and tri-calcium phosphate scaffolds, large numbers of inflammatory cells were observed indicating the invasion of bacteria to the femoral defect. Moreover, for the scaffold containing copper, although the bacteria were less, the potency of copper ions was not strong enough to solve the problem. The synergistic effect of PTT and copper release was found to prevent bacteria from causing serious infection to the defect site (Fig. 10(B)–(D)).[169] Nitric oxide therapy is a combinational approach which improves the efficacy of traditional anticancer therapies by making the cancer cells more susceptible to damage and death. Moreover, it can directly affect the cancer cells and prevent the growth and progression of cancer.[170,171] An innovative synthesis strategy was combined with 3D printing to come up with a multifunctional scaffold for simultaneous bone cancer therapy and regeneration. This study has taken advantage of nitric oxide therapy to not only improve the efficacy of anticancer activity, but also bone regeneration. At first, 2D Nb_2C MXene nanosheets were coated with a mesoporous silica shell.[172] Mesoporous structure relates to the porous texture in the range of 2–50 nm which is considered as suitable for drug loading and controlled release. Moreover, the high surface area of mesoporous materials makes them appropriate candidates for a wide variety of surface functionalities.[173] The surfactant or surface directing agent, which was used to produce the mesoporous silica shell, was cetyltrimethylammonium chloride solution and then the surface of silica was modified with a nitric oxide donor called *S*-nitrosothiol (Fig. 10(E)-I). Next, bioactive glass scaffolds were fabricated through the 3D printing technique and the MXenes were deposited on the surface of scaffold *via* dip coating. Within the initial stages of implantation, the surface modified scaffold was found to increase the temperature of the surrounding microenvironment at a fast rate owing to the high photothermal conversion of 2D Nb_2C within the second NIR biowindow, which along with the high release rate of nitric oxide from the mesoporous structure led to strong antitumor performance (Fig. 10(E)-II). Gradually, the liberation rate of nitric oxide got slower which was found to improve angiogenesis and bone tissue regeneration. Notably, the substrate was bioactive glass composed of silica, calcium oxide, and phosphate and all of them could contribute to accelerated bone tissue repair (Fig. 10(E)-III). To assess the anticancer activity *in vivo*, an ectopic osteosarcoma model was developed and the experiments related to bone regeneration were performed separately in a cranial defect model. The scaffolds endowed with the combination of gas therapy and PTT could successfully eliminate the tumors after 2 weeks without recurrence. The bone regeneration and neovascularization were monitored after 16 weeks through micro-computed tomography and micro-angiography. The results showed that better bone regeneration, degradation, and angiogenesis were observed for the surface-modified scaffolds compared to unmodified ones (Fig. 10(F)–(K)). The release of niobium ions along with low concentration of nitric oxide played a combinatory role in triggering neovascularization and bone repair due to their interconnected and independent mechanisms.[172]

Jaw bone defects generally result from trauma, tumors, maxillofacial infection, *etc.* and the strategies to address these defects are still challenging due to the irregular shapes of these defects. Of course, autologous bone transplantation, as the gold standard of filling up these defects, is the first solution, but this strategy is with some problems including donor site injury, limited supply, pain, *etc.* Nevertheless, the high infection rate is another problematic issue revolving around bone defects, and systemic administration of antibiotics in high dosages is accompanied with cytotoxic effects along with developing bacterial resistance.[174] To repair mandibular defects, a multifunctional 3D printed scaffold was designed that not only provided a microenvironment for bone regeneration, but also eradicated bone infection. On one side, Ti_3C_2 MXene nanosheets were fabricated and on the other side, sodium alginate was mixed with berberine, a natural compound with antibacterial and anticancer activities. Next, biphasic calcium phosphate was added to the mixture of polymer and berberine, and eventually, the MXene nanosheets were added to the bio-ink. In here, the concentrations of biphasic calcium phosphate (BCP) and MXene could directly affect the viscosity of the ink. In other words, the addition of MXene led to the production of more viscous bioinks; however, they still showed the capability of continuous printing. Once the printing was performed, the scaffolds were exposed to calcium chloride for ionic crosslinking which led to desirable mechanical properties for bone reconstruction. Owing to the high photothermal conversion efficacy of MXene nanosheets, laser irradiation leads to heat generation (controllable hyperthermia) and bacterial elimination along with facilitating the release of berberine, which further improved the antibacterial activity and osteogenesis. The printability of different bio-inks was tested through fiber formation, where the bio-ink with a lower amount of calcium phosphate tended to form droplets, while an increase in the ceramic content was synchronized with stabilization of fibers and prevention of fiber breaking once the layer was formed. However, a further increase in the ceramic content caused a discontinuous extrusion resulting from the clogging of the needle. Noteworthily, the addition of both MXene nanosheets and berberine had a negligible effect on the printability of bio-inks. The potential of this scaffold was tested *in vivo* in the infected mandibular defects of rabbits. The samples with and without MXene nanosheets were implanted and laser irradiation was applied on the defect. Sample incorporating the nanosheets experienced an increase in the local temperature from 34 to 50.6 °C, whereas the counterpart could only experience an increase up to nearly 41 °C, demonstrating the high photothermal conversion ability of MXenes. After a week, it was

observed that the defect filled up with MXene-free scaffold was with abscesses and tissue swelling, whereas the high temperature owing to the MXenes led to the elimination of bacteria with minor swelling.[91]

Peripheral nerve injury is among the most common injuries related to the nervous system and it is estimated that about 3 million patients suffer from this problem annually in Europe and about 2 million in USA.[175,176] This injury is a clinical challenge when it exceeds 5 mm in size, and generally, autologous nerve transplantation is considered as the gold standard, but it suffers from donor area damage and inadequate nerve source.[177,178] Therefore, new therapeutic approaches are of particular interest to address these challenges. As an alternative strategy, artificial nerve guidance conduits have attracted considerable attention; they serve as a physical bridge connecting distal and proximal nerve stumps and stimulate the axons' growth and regeneration.[179] With the aid of 4D printing a novel nerve conduit with microchannel guidance was developed which was comprised of poly(L-lactide-*co*-trimethylene carbonate) and single-layer MXene $Ti_3C_2T_x$ nanosheets (Fig. 11(A)). The nerve conduit designed in this study was endowed with a shape memory function capable of changing its shape to a tubular structure once being exposed to body temperature (37 °C); this feature allows the conduit to securely wrap the

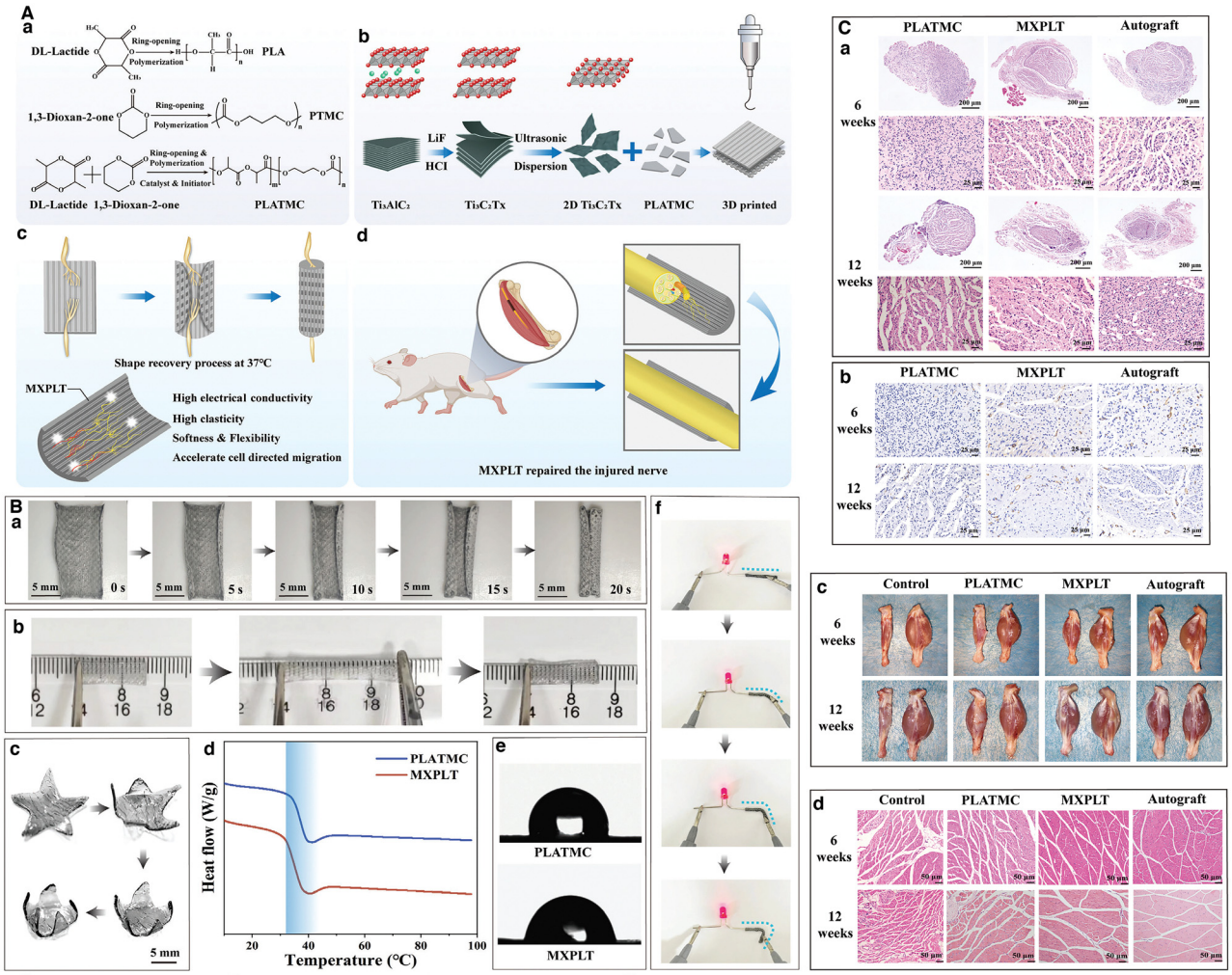

Fig. 11 Development of a MXene-based composite with a shape memory function for peripheral nerve injuries. (A) (a) Chemical formula of different compositions used to prepare the composite; (b) preparation of 2D MXene nanosheets followed by incorporation with poly(L-lactide-*co*-trimethylene carbonate) for 3D printing of the composite; (c) and (d) schematic illustration of sciatic nerve regeneration with the composite; this material can be curled and wrapped once being exposed to body temperature; the microstructure conducts electrical signals efficiently and improves the regeneration rate of nerve cells. (B) (a) From left to right, the dynamic change of the composite at 37 °C after 0, 5, 10, 15, and 20 s; (b) stretching capability of the composite; (c) 4D-printed composite in the form of a five-point star which changes its morphology on exposure to temperature; (d) DSC curves of poly(L-lactide-*co*-trimethylene carbonate) and the composite; (e) wettability of the composite and poly(L-lactide-*co*-trimethylene carbonate); (f) testing the electrical conductivity of the composite by lighting up an LED under flat and different bending states. (C) (a) and (b) H&E staining and CD31 staining in the cross-section of sciatic nerve treated with different samples after 6 and 12 weeks of treatment. (c) Gross images and H&E staining of the gastrocnemius muscle after 6 and 12 weeks of *in vivo* experiments. Abbreviations: PLATMC, poly(L-lactide-*co*-trimethylene carbonate); MXPLT, MXene-incorporated poly(L-lactide-*co*-trimethylene carbonate). Reproduced with permission from ref. 180. Copyright 2024, Wiley.

broken stumps of the injured nerve automatically once implanted in the defect area (Fig. 11(B)). It is known that muscle movement causes deformation in the nerves and this shape memory composite with high ductility and elasticity could withstand the deformation. The microchannels introduced in the structure of the composite were found to stimulate and accelerate cell migration during the regeneration process. Speaking of the MXene nanosheets, they endowed the composite with electrical conductivity which is of great importance to form a complete electrical pathway during the nerve regeneration process. *In vivo* experiments were performed successfully on a Sprague-Dawley rat model by introducing a 10 mm sciatic nerve defect. 4D printed composites were grafted in the defected rat model, while the rats not receiving the graft treatment were considered as the negative control. Noteworthily, the rats treated with the autograft were regarded as the positive control. 6 and 12 weeks after the surgery, the nerve repair was tracked, and it turned out that the composite-grafted implant and the autograft improved the regeneration significantly, whereas the negative control failed to do so. The composite was observed to wrap around the damaged nerve indicating the protective role of biomaterials even after 12 weeks post-implantation. It is worth mentioning that the material underwent degradation, and its size reduced from the 6^{th} week till the 12^{th} week. The histological analysis performed on the muscle fibers and their diameters showed that after 6 weeks of implantation, the defects treated with the autografts outperformed the others while the control had the smallest fiber diameter along with muscle atrophy. Even after 12 weeks, the autograft was still the best. The defects treated with the composite also experienced a significant better regeneration rate after 12 weeks (Fig. 11(C)).[180]

The combination of 3D-printing technologies with MXenes is synchronized with giving birth to multifunctional biomaterials for a wide variety of biomedical applications. One of these areas is tissue engineering scaffolds; MXenes with great electrical conductivity are incorporated in 3D-printed scaffolds for cardiac and neural tissue engineering. By mimicking the electrical properties of natural tissues, the promotion of the growth and differentiation of cardiomyocytes and neurons takes place. MXenes are known to induce antibacterial activity by releasing antibacterial ions like Ti^{4+} or inducing photothermal/photodynamic therapies (PTT/PDT). The platforms surface-modified with MXenes or incorporating MXenes can prevent infection, which is known as a critical factor in the success of implanted biomaterials. The high surface area and surface chemistry of MXenes are two great properties for designing smart drug delivery carriers responsive to internal and/or external stimuli. Moreover, the combination of 3D-printing technology with MXenes enables the customization of drug delivery systems to individual patient need and personalized medicine. Other areas for the application of MXene-based 3D-printed platforms are bio-sensing, cancer therapy, and regenerative medicine. The extraordinary physicochemical properties of MXenes, such as high electrical conductivity, high surface area, tunable surface chemistry, photothermal conversion, *etc.*, give multifunctionality to the 3D-printed platform as a wearable sensor to continuously monitor the physiological parameters (*e.g.* heart rate, blood pressure, *etc.*) or as an anticancer agent. The high photothermal conversion rate of MXenes makes them excellent candidates for PTT and PDT. Regarding regenerative medicine, as discussed throughout the section, MXenes have stimulatory effects on healthy cells and therapeutic roles in preventing infection and/or eradicating cancerous cells. This combination therapy is highly desirable because it opens new doors for patients with complex situations.

3.3.1. Biocompatibility of MXene-based 3D-printed platforms. Speaking of biomedical applications, a biomaterial that is supposed to be in contact with a living tissue requires some essential features.[181] These features are mechanical properties, physical and chemical properties, bioactivity, *etc.* but biocompatibility is a prerequisite. Biocompatible generally refers to a material that can be in contact with a living tissue or a living system without showing toxicity, injuries, or immunological effects. There are key aspects to biocompatibility including non-toxicity (not releasing harmful substances to surrounding cells), non-immunogenicity (not triggering inflammation or rejection by the immune system), stability (chemical stability within the body's environment), and bio-functionality (should perform its intended function).[181,182] Assessment of biocompatibility is performed through different experiments *in vitro* (*e.g.* cell viability, hemocompatibility, genotoxicity, cell adhesion, *etc.*) and *in vivo* (*e.g.* blood test, histological analysis, analyzing urine and feces, *etc.*).[147] MXene-incorporated 3D-printed platforms have been applied in both soft and hard tissue regeneration and cancer therapy. Besides performing different *in vitro* studies spanning from cytotoxicity to cell attachment and angiogenesis, some of these studies have considered the potential of those biomaterials *in vivo*.[91,151,165,169,172,180] A study has applied a monolayer $Ti_3C_2T_x$ nanosheet for both soft and hard tissue regeneration. Through a series of *in vitro* assays, the nanosheets' cytotoxicity, cell migration, and angiogenic behavior were assessed. Different concentrations ranging from 6.25 to 100 μg mL^{-1} with and without NIR were tested against C_2C_{12} and human umbilical vein endothelial cells up to 48 h, no toxic effect was observed. The nanosheets' ability to repair skull defects was tested *in vivo* in a 5 mm skull defect rat model; the microcomputed tomography and histological examinations revealed that new bone tissue appeared around the skull defects after 4 weeks post-implantation without any negative effect. The same material was applied to an infected wound to assess the antibacterial potential and tissue regeneration up to 14 days. The combination of MXenes and NIR had the best performance and completely regenerated the tissue with visible skin appendages and blood vessels analyzed through H&E staining.[151] Ti_3C_2 nanosheets and berberine as a natural medicine were incorporated into 3D-printed biphasic calcium phosphate scaffolds for antibacterial activity and bone regeneration. MC3T3-E1 and rabbit bone mesenchymal stem cells were employed for cytotoxicity and osteogenic differentiation for 7 days; the cells were seeded on the scaffolds. Continuous cell proliferation was observed for all the scaffolds implying excellent cell compatibility of the samples with and without the MXene nanosheets. Through ELISA, the

activity of inflammatory cytokines was assessed, and no significant changes in the activity of tumor necrosis factor-alpha and interleukin-6 were observed, indicating that neither the MXenes nor the scaffold cause inflammation. The *in vivo* experiments were performed on large mandibular defects constructed in New Zealand white rabbits up to 4 months. For the blank groups, which were not treated with any scaffolds, it was difficult for spontaneous regeneration and only a small amount of new bone was visible at the edge of defects after one month. Compared to the bare scaffolds, the one loaded with the MXenes showed better osteogenic properties. H&E and Masson's trichrome staining were performed on the tissue harvested at months 1 and 4; the results exhibited no necrosis and no negative effects on the surrounding tissues of scaffolds.[91] There are a few studies that besides implantation of the platform *in vivo* for therapeutic and/or tissue regeneration purposes have performed in-depth analysis of the long-term toxicity of MXene-based 3D-printed platforms.[165,180] 4D-printed platforms with shape memory features were developed as artificial nerve guidance conduits for large peripheral nerve defects; the platform was composed of poly(L-lactide-*co*-trimethylene carbonate) and $Ti_3C_2T_x$ MXene nanosheets. *In vivo* toxic effects on different organs were assessed 12 weeks post-implantation by analyzing the tissues of the liver, heart, kidney, spleen, and lungs (H&E staining). The histological examinations revealed no abnormalities in these major organs along with no negative toxic effects on the tissues.[180] Another study deposited Ti_3C_2 nanosheets on the 3D-printed bioactive glass scaffolds for simultaneous bone cancer therapy and regeneration. In this study, *in vivo* experiments were performed for 24 weeks along with a detailed long-term toxicity assessment. After 24 weeks, the major organs of rats including heart, spleen, kidney, lung, and liver were dissected followed by fixation in 10% formalin and staining with H&E for histological examinations. Moreover, a blood test was done to measure hematology parameters like erythrocytes, leucocytes, hemoglobin, *etc.* The results indicated that no significant change was observed between the rats treated with the surface-modified scaffolds and the control group. The histological sections of the major organs showed no abnormalities between the samples and the control groups. Therefore, during the long therapeutic/regenerative period, no inflammation, toxicity, or infection was observed implying the biocompatibility of the scaffolds.[165]

3.4. Other applications

In the recent decade, developing microwave absorption materials has attracted special attention because of their importance in human life and military equipment.[183] The traditional ones made of metals, ceramics, and conducting polymers suffer from poor loss property, high density, and narrow absorption frequency due to the single attenuation mechanism.[184] There is also another problem related to microwave absorption materials, which is the stability of these materials in different environments specifically the extreme ones.[185] Therefore, it is of great importance to fabricate new materials capable of attenuating electromagnetic wave through different pathways and also capable of exhibiting diverse environmentally adaptive behavior. A nanocomposite with shape memory feature was designed as an advanced microwave absorption material. Two types of nanofillers were introduced in the structure of the polymer matrix including ZIF 67-deposited MXene nanosheets and Ni- zeolitic imidazolate frameworks (ZIF) 67-deposited carbon nanotubes, which were prepared through the *in situ* growth and pyrolysis. The homogeneous distribution of the nanofillers in the polymer matrix endowed the nanocomposite with a rigid-flexible nature, strong interface bonding, bi-continuous phase separation structure, and multidimension characteristics. Through direct ink writing, the complex 3D-printed shapes were fabricated and exposed to microwave irradiation to enhance the mechanical and shape-retention properties. Moreover, the 3D-printed objects showed photothermal-induced shape memory performance by which their shape can be manipulated by light irradiation. Speaking of environmental adaptability, the nanocomposite was found to possess excellent mechanical properties, long-term anti-corrosion ability, super-amphiphobicity, and flame-retardancy.[186]

Shape memory materials are related to smart materials changing shape when a specific stimulus is applied.[187] These materials are beneficial and usually used in 4D-printed structures owing to their rapid actuation and large deformation potential; these unique features provide an opportunity for a wide variety of applications—spacecraft, solar sails, temporary architectures, deployable antennas, *etc.*[188,189] The mechanism of action behind this behavior is related to the shape memory effect; these materials can hold a temporary position attributed to their hard-crystalline phase, whereas their amorphous structure allows for the recovery to the temporary position, which is reversible, upon applying a stimulus such as heat. The temperature, which is the reason for recovery, is at or above the polymer glass transition temperature providing a situation by which the polymer switches from a stiff to a soft state.[190] Using thermoplastic polyurethane and poly(lactic acid), a shape memory polymer composite incorporating MXene (Ti_3C_2) flakes was fabricated. The MXene nanosheets were added to the polymer matrix at different concentrations and 0.5 wt% turned out to yield the composite with enhanced thermal, mechanical, and morphological properties. Increasing the MXene's content up to 2 wt% contributed to a superb shape memory effect leading to a fast recovery to 98% of its original status in less than 14 s. The shape memory effect in pristine and MXene-incorporated samples was assessed and is indicated in Fig. 12(A). The combination of polyl(actic acid) and thermoplastic polyurethane resulted in an optimal shape memory performance; the former has a highly crystalline structure acting as a fixing domain and the polyurethane with its amorphous structure plays the switching domain's role. By increasing the amount of MXene in the polymer matrix, the recovery time got faster compared to the sample without the MXene flakes. The reason why such a phenomenon was observed has been attributed to the effect of MXene flakes on the polyurethane; the flakes improved the connection between polyurethane spheres and created a more robust and continuous phase that greatly enhanced the material's recovery rate. Different structures

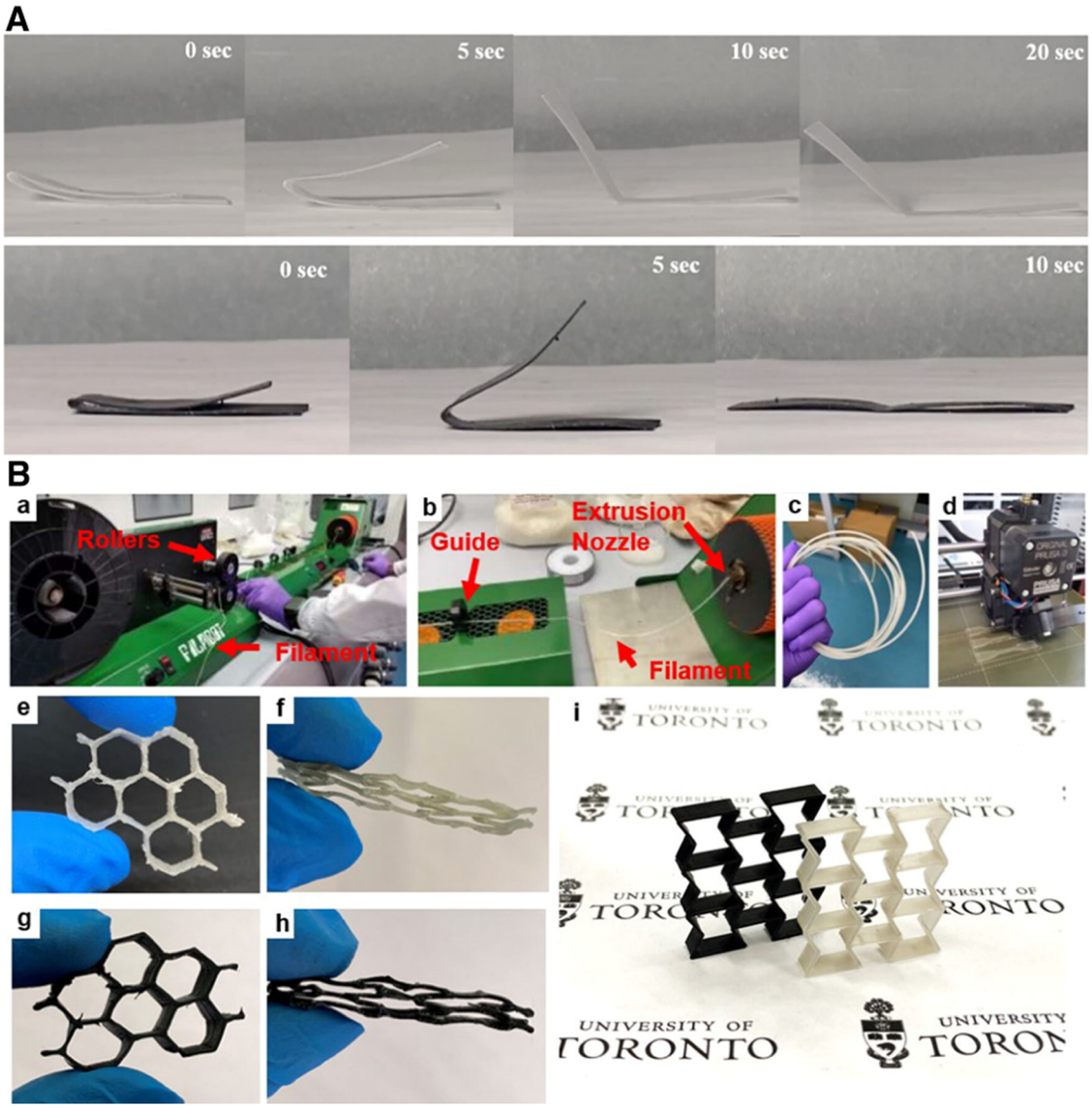

Fig. 12 4D-printed MXene-incorporated composites for deployable actuating structures. (A) Shape memory performance of the samples without and with MXene flakes (2 wt%) at different time intervals. (B) 4D printing of different samples including (a) and (b) filament extrusion procedure, (c) extruded filament and (d) the process of fabrication of the shape memory polymer composite filaments. (e) and (f) The honeycomb structure without MXenes in the normal and deformed states. (g) and (h) The honeycomb structure with MXenes (2 wt%) in the normal and deformed states. (i) The 4D-printed auxetic structures with and without MXenes. Reproduced with permission from ref. 191. Copyright 2022, American Chemical Society.

including honeycomb and auxetic were printed to see the potential of 4D printed samples in changing the shape followed by recovery time (Fig. 12(B)). The samples indicated excellent fixing and a fast recovery rate without cracking. Once the samples were exposed to 80 °C in an oven, they completely recovered themselves. However, after applying a few deformations, the recovery became less complete showing that frequent deformation causes damage to the structure.[191]

4. Challenges and future directions

Emerging 4D printing approaches add an extra dimension of time to the manufacturing process, enabling dynamic transformations in response to external stimuli. This novel approach enables the creation of materials and structures that can adapt, change shape, or exhibit dynamic behaviors in response to external stimuli. By integrating smart materials with programmable properties, such as shape memory alloys, hydrogels, or responsive polymers, 4D printing opens up a realm of possibilities for advanced manufacturing applications.[39,40,43,75] One of the key advantages of 4D printing is the ability to produce adaptive materials and structures that can self-assemble, reconfigure, or respond to environmental changes.[39] By leveraging the inherent properties of smart materials, such as their ability to undergo reversible phase transitions or shape transformations, 4D printing enables the creation of dynamic components with tailored functionalities.

Table 2 Some salient advantages/benefits of 3D/4D printing of MXenes and their composites

	3D printing	4D printing
1	Customization: 3D printing enables the precise and tailored fabrication of MXene-based structures, allowing for customized designs to meet specific application requirements[82]	Dynamic adaptability: 4D printing with MXenes enables structures to dynamically adapt and respond to external stimuli, offering enhanced functionality and versatility[37]
2	Complex geometries: with 3D printing, intricate and complex geometries can be easily achieved with MXene materials, expanding the possibilities for innovative designs[82]	Self-assembly: MXenes in 4D printing can facilitate self-assembly of components, reducing the need for complex assembly processes and enhancing efficiency[76]
3	Material efficiency: the additive nature of 3D printing minimizes material waste, making it a more sustainable option for utilizing MXenes effectively[82]	Responsive properties: MXenes exhibit responsive properties in 4D printing, allowing for structures to change shape, stiffness, or other characteristics based on specific triggers[37]
4	Rapid prototyping: 3D printing with MXenes facilitates quick prototyping of devices and components, accelerating the development cycle and reducing time-to-market[195]	Multifunctionality: the integration of MXenes in 4D printing enables the development of multifunctional structures with capabilities beyond traditional static materials[77]
5	Integration of multiple materials: 3D printing technology allows for the incorporation of different materials alongside MXenes, enabling the creation of multifunctional and composite structures[82]	Smart material applications: MXenes in 4D printing are ideal for smart material applications, where adaptive and programmable features are required for various industries[37]
6	Cost-effective production: by streamlining the manufacturing process, 3D printing of MXenes can lead to cost savings in the production of advanced devices and components[82]	Enhanced design possibilities: 4D printing with MXenes opens up new design possibilities, enabling the creation of complex, interactive structures with unique properties[37,196]
7	Enhanced performance: the precise control offered by 3D printing enhances the performance of MXene-based materials, optimizing their properties for various applications[197]	Improved performance: the dynamic nature of MXenes and performance of 4D printing can lead to improved performance in terms of energy storage, sensing capabilities, and other functional aspects[76,198]
8	Design flexibility: with 3D printing, designers have the flexibility to iterate and modify MXene structures easily, fostering innovation and experimentation in material design[82]	Innovative applications: MXenes in 4D printing facilitate the development of innovative applications in fields such as biomedical devices, soft robotics, and advanced engineering solutions[42,199]

These adaptive structures hold great promise for application in areas such as aerospace, healthcare, and robotics, where dynamic performance is critical.[192] Another significant aspect of 4D printing is the programmable nature of the printed objects. Through precise control of material composition, design parameters, and external stimuli, designers can impart specific functionalities to printed components. This programmability allows for the creation of complex geometries, tunable mechanical properties, and responsive behaviors in printed structures. By harnessing the capabilities of smart materials in conjunction with advanced printing techniques, 4D printing offers a pathway to developing customized products with unique properties and behaviors.[193,194] Some of the important advantages/benefits as well as challenges/limitations of 3D/4D printing of MXenes and their composites are summarized in Tables 2 and 3.

Generally speaking, MXene-based 3D-printed platforms have been prepared in two different ways—incorporation in the structure and deposition on the surface of the platform. Each technique has its pros and cons based on the desired application. The advantages of MXene-incorporated structures are the uniform distribution of nanosheets throughout the platform, improved properties of the platform (*e.g.* mechanical, electrical, thermal, *etc.*), strong bonding which leads to better structural integrity, and a single-step process yielding the final product after the printing process. On the other hand, post-printing surface functionalization has some specific benefits for some applications. For instance, the deposited nanosheets on the surface can induce PTT/PDT once they are exposed to the biological environment in the case of those biomedical applications that require a fast response (*e.g.* infection, *etc.*). The advantages of this technique are as follows: surface functionalization, especially for applications requiring specific surface properties; targeted application, MXenes can be intentionally deposited on specific areas of a scaffold for more targeted functionality; flexibility in scaffold material, this technique is versatile and can be applied in various 3D-printed scaffolds without worrying about the compatibility of materials during the printing process; and post-processing optimization, the properties of deposited MXenes can be optimized post-printing, which provides better control over the final characteristics.

Overall, one of the primary challenges in the realm of 3D/4D printing of MXene-based composites lies in the intricate balance between achieving high-performance material properties and optimizing the manufacturing processes for scalability and cost-effectiveness. The synthesis of MXene materials at a large scale while maintaining their exceptional properties poses a significant hurdle that researchers and engineers need to overcome. Additionally, ensuring the compatibility of MXenes with existing 3D/4D printing technologies, along with addressing issues related to material consistency, printing resolution, and post-processing requirements, presents a multifaceted challenge that requires innovative solutions and interdisciplinary collaboration to drive the field of additive manufacturing forward.

4.1. Dispersion optimization

A key challenge in the utilization of MXene nanosheets in additive manufacturing is the effective dispersion within printing matrices. Achieving a uniform distribution of MXene nanosheets throughout the material is crucial to ensure consistent material properties and structural integrity. Overcoming issues related to agglomeration and poor dispersion remains a

Table 3 Some important challenges/limitations of 3D/4D printing of MXenes and their composites

	3D printing	4D printing
1	Material selection: limited availability of MXene powders with suitable properties for 3D printing can restrict material options and hinder the optimization of printed structures[34,200]	Complexity in design: designing MXene-based structures for 4D printing can be intricate and require advanced knowledge of material behavior and stimuli-responsive properties, potentially limiting accessibility for some users[44,201]
2	Printed structural integrity: achieving consistent structural integrity and homogeneity in 3D printed MXene objects can be challenging, leading to potential defects or weak points[82]	Control and calibration: achieving precise control over the stimuli-responsive behavior of MXenes in 4D printing may pose challenges, necessitating meticulous calibration for desired outcomes[77,202]
3	Post-processing requirements: post-processing steps such as curing, sintering, or surface treatments may be necessary for enhancing the mechanical properties of 3D printed MXene components, adding complexity to the manufacturing process[82]	Material compatibility: ensuring compatibility between MXene materials and the 4D printing process, including solvents, inks, and printing conditions, is crucial but may require extensive testing and optimization[37,193]
4	Resolution constraints: the resolution limitations of 3D printing technologies may impact the level of detail and intricacy that can be achieved in MXene-based prints, limiting design possibilities[203]	Durability and longevity: the long-term durability and stability of MXene-based structures produced through 4D printing ought to be investigated, especially in applications requiring prolonged functionality[39]
5	Cost considerations: the cost of acquiring MXene materials and specialized 3D printing equipment, as well as the need for skilled operators, can present financial barriers to widespread adoption[204]	Scalability issues: scaling up production of 4D printed MXene components for commercial use can be complex and may require substantial investment in equipment, processes, and quality control measures[205]
6	Scale-up challenges: scaling up production of 3D printed MXene components for industrial applications may pose challenges in terms of consistency, quality control, and manufacturing efficiency[205]	Processing time: the time required for MXene structures to respond to stimuli and undergo shape changes in 4D printing may vary, impacting the overall production efficiency and speed[37,198]
7	Material properties: variability in MXene properties, such as conductivity, mechanical strength, and stability, can affect the performance of 3D printed parts and require thorough characterization[82]	Integration challenges: integrating MXenes with other materials or components in 4D printing setups can present challenges in achieving seamless transitions and functional interfaces between different elements[43,194]
8	Environmental impact: the environmental impact of 3D printing processes, including energy consumption and waste generation, is a consideration in the sustainable production of MXene-based products[206]	Regulatory compliance: meeting regulatory standards and safety requirements for MXene-based 4D printed products may involve additional testing, validation, and compliance measures, adding complexity to the development process[207]

significant hurdle in maximizing the performance of MXene-based composites.

4.2. Structural uniformity

Another critical challenge lies in ensuring the structural uniformity of printed components. Variations in layer adhesion, surface finish, and dimensional accuracy can arise due to inconsistencies in the printing process, affecting the overall quality of the final product. Enhancing the structural uniformity of printed objects is essential for realizing the full potential of MXene-based materials in additive manufacturing applications.

4.3. Scalability and production efficiency

Scaling up the production of MXene-based composites for industrial applications poses a considerable challenge. Optimizing production processes to meet the demands of large-scale manufacturing while maintaining cost-effectiveness is essential. Addressing issues related to process efficiency, material wastage, and production scalability is crucial for the widespread adoption of MXene materials in additive manufacturing on an industrial scale.

4.4. Material compatibility and integration

Ensuring compatibility between MXene nanosheets and the printing matrix is a critical aspect that presents challenges in achieving desired material properties. The selection of suitable matrix materials, processing conditions, and post-processing techniques plays a significant role in optimizing the integration of MXenes into additive manufacturing processes. Overcoming compatibility issues and enhancing the integration of MXene nanosheets with printing matrices are key challenges in advancing the application of these materials in 3D/4D printing technologies.

The future of 3D/4D printing of MXene-based composites holds immense promise for revolutionizing various industries and advancing the field of additive manufacturing. As researchers continue to explore the capabilities of MXenes in dynamic printing processes, several exciting perspectives emerge that could shape the future of material design and technology. One key future perspective is the development of multifunctional MXene composites with tailored properties for specific applications. By fine-tuning the composition and structure of MXene-based materials, researchers can create advanced composites that exhibit a combination of mechanical strength, electrical conductivity, thermal stability, and responsiveness to external stimuli. These multifunctional materials have the potential to drive innovation in fields such as aerospace, healthcare, and electronics. Another future perspective is the integration of artificial intelligence (AI) and machine learning algorithms in the design and optimization of MXene-based composites for 3D/4D printing. By leveraging AI-driven tools, researchers can accelerate the material discovery process, predict the performance of printed objects, and optimize printing parameters for enhanced efficiency and quality. This synergy between advanced computational tools and additive manufacturing techniques could lead to the rapid development of novel materials with unprecedented properties. Furthermore,

the advent of bio-inspired design principles in 3D/4D printing of MXene composites opens up possibilities for creating biomimetic structures with self-healing, self-assembling, or shape-morphing capabilities. Drawing inspiration from nature, researchers can mimic the complexity and adaptability of biological systems to design materials that exhibit remarkable functionalities in response to environmental cues.

5. Conclusion

The intersection of 3D/4D printing with MXenes and their composites represents a transformative frontier in materials science and additive manufacturing. The unique properties of MXenes, such as high conductivity, mechanical strength, and responsiveness to stimuli, coupled with the precision and adaptability of 3D/4D printing technologies offer unprecedented opportunities for creating advanced materials with tailored properties and functionalities. The emerging applications of MXene-based composites in diverse industries, including healthcare, electronics, energy storage, and aerospace, showcase the potential impact of these materials in revolutionizing traditional manufacturing processes and enabling the development of innovative products with enhanced performance and versatility. As research progresses and technology evolves, the future of 3D/4D printing of MXene-based composites holds promise for pushing the boundaries of material design and engineering. By exploring new avenues in multifunctional material development, incorporating AI in material optimization, and drawing inspiration from nature for biomimetic designs, researchers can drive forward the field of additive manufacturing towards creating intelligent, adaptive, and sustainable materials.

Despite the promising potential of 3D/4D printing of MXene-based composites, several challenges and limitations exist that need to be addressed to fully realize their benefits in advanced manufacturing. One of the primary challenges is the scalability of production and the cost-effectiveness of MXene materials. As the demand for high-performance additive manufacturing materials grows, ensuring the sustainable and economical synthesis of MXenes at a large scale poses a significant hurdle for widespread adoption. Additionally, the integration of MXenes into existing 3D/4D printing technologies requires further research and development to optimize printing parameters, enhance material compatibility, and improve printing resolution. Achieving precise control over the microstructure and properties of MXene composites during printing processes remains a technical challenge that needs to be overcome to unlock the full potential of these materials in additive manufacturing. Looking towards the future, one of the key perspectives is the exploration of novel applications and functionalities of MXene-based composites in emerging fields such as wearable technology, soft robotics, and environmental sensing. However, it is essential to acknowledge the current limitations of MXene-based composites, including issues related to environmental impact, recycling, and end-of-life disposal. Addressing these sustainability concerns and developing environmentally friendly manufacturing processes for MXenes are crucial steps towards ensuring the long-term viability and ethical use of these advanced materials in additive manufacturing. By embracing a holistic approach that considers both technological advancements and ethical considerations, the future of 3D/4D printing of MXene-based composites can pave the way for a more sustainable and innovative manufacturing landscape.

Author contributions

Ashkan Bigham: writing – review & editing; Atefeh Zarepour: writing– review & editing; Arezoo Khosravi: visualization, writing – review & editing; Siavash Iravani: supervision, conceptualization, writing – review & editing; Ali Zarrabi: supervision, writing – review & editing.

Data availability

No data was used for the research described in the article.

Conflicts of interest

The authors declare no conflict of interest.

References

1 D. Khorsandi, D. Rezayat, S. Sezen, R. Ferrao, A. Khosravi, A. Zarepour, M. Khorsandi, M. Hashemian, S. Iravani and A. Zarrabi, *J. Mater. Chem. B*, 2024, **12**, 4584–4612.
2 S. F. Iftekar, A. Aabid, A. Amir and M. Baig, *Polymers*, 2023, **15**, 2519.
3 M. H. Mobarak, M. A. Islam, N. Hossain, M. Z. Al Mahmud, M. T. Rayhan, N. J. Nishi and M. A. Chowdhury, *Appl. Surf. Sci. Adv.*, 2023, **18**, 100462.
4 H. Liu, L. He, M. Kuzmanović, Y. Huang, L. Zhang, Y. Zhang, Q. Zhu, Y. Ren, Y. Dong, L. Cardon and M. Gou, *Small Methods*, 2024, **8**, 2301121.
5 M. N. Nadagouda, M. Ginn and V. Rastogi, *Curr. Opin. Chem. Eng.*, 2020, **28**, 173–178.
6 M. A. S. R. Saadi, A. Maguire, N. T. Pottackal, M. S. H. Thakur, M. M. Ikram, A. J. Hart, P. M. Ajayan and M. M. Rahman, *Adv. Mater.*, 2022, **34**, 2108855.
7 M. Manoj Prabhakar, A. K. Saravanan, A. Haiter Lenin, I. Jerin leno, K. Mayandi and P. Sethu Ramalingam, *Mater. Today: Proc.*, 2021, **45**, 6108–6114.
8 S. Shinde, R. Mane, A. Vardikar, A. Dhumal and A. Rajput, *Eur. Polym. J.*, 2023, **197**, 112356.
9 Z. Guan, L. Wang and J. Bae, *Mater. Horiz.*, 2022, **9**, 1825–1849.
10 M. A. Alhnan, T. C. Okwuosa, M. Sadia, K.-W. Wan, W. Ahmed and B. Arafat, *Pharm. Res.*, 2016, **33**, 1817–1832.
11 T. Chu, S. Park and K. Fu, *Carbon Energy*, 2021, **3**, 424–439.
12 R. Akhter and S. S. Maktedar, *J. Materiomics*, 2023, **9**, 1196–1241.

13 B. Anasori and Y. Gogotsi, *Graphene 2D Mater.*, 2022, **7**, 75–79.
14 D. Ayodhya, *Diamond Relat. Mater.*, 2023, **132**, 109634.
15 B. Fu, J. Sun, C. Wang, C. Shang, L. Xu, J. Li and H. Zhang, *Small*, 2021, **17**, 2006054.
16 U. U. Rahman, M. Humayun, U. Ghani, M. Usman, H. Ullah, A. Khan, N. M. El-Metwaly and A. Khan, *Molecules*, 2022, **27**(15), 4909.
17 R. M. Ronchi, J. T. Arantes and S. F. Santos, *Ceram. Int.*, 2019, **45**, 18167–18188.
18 L. Li and G. Shen, *Mater. Horiz.*, 2023, **10**, 5457–5473.
19 N. Kitchamsetti and A. L. F. de Barros, *ChemCatChem*, 2023, **15**, e202300690.
20 L. Verger, C. Xu, V. Natu, H.-M. Cheng, W. Ren and M. W. Barsoum, *Curr. Opin. Solid State Mater. Sci.*, 2019, **23**, 149–163.
21 J. Lu, G. Zhu, S. Wang, C. Wu, X. Qu, X. Dong, H. Pang and Y. Zhang, *Small*, 2024, 2401565.
22 K. A. S. Usman, S. Qin, L. C. Henderson, J. Zhang, D. Y. Hegh and J. M. Razal, *Mater. Horiz.*, 2021, **8**, 2886–2912.
23 N. Liu, J. Yuan, X. Zhang, Y. Ren, F. Yu and J. Ma, *Mater. Horiz.*, 2024, **11**, 1223–1233.
24 R. Ibragimova, P. Erhart, P. Rinke and H.-P. Komsa, *J. Phys. Chem. Lett.*, 2021, **12**, 2377–2384.
25 M. Mozafari and M. Soroush, *Mater. Adv.*, 2021, **2**, 7277–7307.
26 B. Anasori, M. R. Lukatskaya and Y. Gogotsi, *Nat. Rev. Mater.*, 2017, **2**, 16098.
27 Z. Xiao, X. Xiao, L. B. Kong, H. Dong, X. Li, X. Sun, B. He, S. Ruan and J. Zhai, *J. Materiomics*, 2023, **9**(6), 1067–1112.
28 G. Zhou, X. Liu, C. Liu, Z. Li, C. Liu, X. Shi, Z. Li, C. Mei and M.-C. Li, *J. Mater. Chem. A*, 2024, **12**, 3734–3744.
29 Y. I. Jhon and J. H. Lee, *Comput. Mater. Sci.*, 2023, **227**, 112268.
30 B. C. Wyatt, A. Rosenkranz and B. Anasori, *Adv. Mater.*, 2021, **33**, 2007973.
31 C. C. Leong, Y. Qu, Y. Kawazoe, S. K. Ho and H. Pan, *Catal. Today*, 2021, **370**, 2–13.
32 Y. Sun, X. Meng, Y. Dall'Agnese, C. Dall'Agnese, S. Duan, Y. Gao, G. Chen and X. F. Wang, *Nano-Micro Lett.*, 2019, **11**, 1–22.
33 S. Iravani and R. S. Varma, *Molecules*, 2022, **27**, 6939.
34 A. Salas, H. Pazniak, J. Gonzalez-Julian, S. Bianco, J. Amici, T. Ouisse, I. Roppolo and M. Cocuzza, *Composites, Part B*, 2023, **263**, 110854.
35 D. Ji, J. Liu, J. Zhao, M. Li, Y. Rho, H. Shin, T. H. Han and J. Bae, *Nat. Commun.*, 2024, **15**, 3925.
36 M. R. Manshor, Y. A. Alli, H. Anuar, O. Ejeromedoghene, E. O. Omotola and J. Suhr, *Mater. Sci. Eng., B*, 2023, **295**, 116567.
37 K. McLellan, T. Li, Y.-C. Sun, M. B. Jakubinek and H. E. Naguib, *ACS Appl. Polym. Mater.*, 2022, **4**, 8774–8785.
38 P. Srinivas, L. Jacob, M. Shebeeb C, H. Butt, I. Barsoum, R. K. Abu Al-Rub and W. Zaki, *Adv. Eng. Mater.*, 2024, **26**, 2301698.
39 A. Ahmed, S. Arya, V. Gupta, H. Furukawa and A. Khosla, *Polymer*, 2021, **228**, 123926.
40 P. Cataldi, M. Liu, M. Bissett and I. A. Kinloch, *Adv. Mater. Technol.*, 2022, **7**, 2200025.
41 M. Jakubczak, D. Bury, A. Wojciechowska, J. Mitrzak, K. Budnik, D. Moszczyńska and A. M. Jastrzębska, *J. Alloys Compd.*, 2024, **976**, 173318.
42 M. Das, R. S. Ambekar, S. K. Panda, S. Chakraborty and C. S. Tiwary, *J. Mater. Res.*, 2021, **36**, 4024–4050.
43 X. Wan, Z. Xiao, Y. Tian, M. Chen, F. Liu, D. Wang, Y. Liu, P. J. Da Silva Bartolo, C. Yan, Y. Shi, R. R. Zhao, H. J. Qi and K. Zhou, *Adv. Mater.*, 2024, 2312263.
44 S. Iravani and R. S. Varma, *Nano-Micro Lett.*, 2024, **16**, 142.
45 J. Zhang, Q. Hu, S. Wang, J. Tao and M. Gou, *Int. J. Bioprint.*, 2020, **6**, 242.
46 Y. Hu, J. Gu, Y. Zhang, G. Liu, X. Yi and X. Liu, *Compos. Commun.*, 2024, **48**, 101953.
47 B. Huang, Z. Zhou, L. Wei, Q. Song, W. Yu, Y. Zhou, R. Hu, W. Zhang and C. Lu, *Composites, Part B*, 2021, **225**, 109261.
48 L. Chen, B. Huang, F. Wei, X. Guo, D. Zhang, K. Thummavichai, D. Chen, N. Wang and Y. Zhu, *ACS Appl. Polym. Mater.*, 2023, **5**, 9852–9864.
49 A. Duongthipthewa, H. Zhou, Q. Wang and L. Zhou, *Composites, Part B*, 2024, **270**, 111108.
50 X.-Y. Yin, Y. Zhang, X. Cai, Q. Guo, J. Yang and Z. L. Wang, *Mater. Horiz.*, 2019, **6**, 767–780.
51 A. Fontana-Escartín, S. Lanzalaco, O. Bertran, D. Aradilla and C. Alemán, *Colloids Surf., A*, 2023, **671**, 131632.
52 C. Dai, H. Lin, G. Xu, Z. Liu, R. Wu and Y. Chen, *Chem. Mater.*, 2017, **29**, 8637–8652.
53 W. Luo, H. Liu, X. Liu, L. Liu and W. Zhao, *Colloids Surf., B*, 2021, **201**, 111631.
54 L. Wang, D. P. Wang, K. Wang, K. Jiang and G. Shen, *ACS Mater. Lett.*, 2021, **3**, 921–929.
55 X. Xu, T. Guo, M. Lanza and H. N. Alshareef, *Matter*, 2023, **6**, 800–837.
56 Y. Zhang, M. Gong and P. Wan, *Matter*, 2021, **4**, 2655–2658.
57 W. Huang, X. Liu, Y. Zhou, S. Yang, W. Huang, Z. Chen, J. Feng, Z. Chen, X. Li and X. Gui, *ACS Appl. Nano Mater.*, 2024, **7**, 15308–15316.
58 K. Li, M. Liang, H. Wang, X. Wang, Y. Huang, J. Coelho, S. Pinilla, Y. Zhang, F. Qi, V. Nicolosi and Y. Xu, *Adv. Funct. Mater.*, 2020, **30**, 2000842.
59 X. Li, Z. Huang, C. E. Shuck, G. Liang, Y. Gogotsi and C. Zhi, *Nat. Rev. Chem.*, 2022, **6**, 389–404.
60 D. Parajuli, N. Murali, D. KC, B. Karki, K. Samatha, A. A. Kim, M. Park and B. Pant, *Polymers*, 2022, **14**, 3433.
61 L. Sun, H. Wang, S. Zhai, J. Sun, X. Fang, H. Yang, D. Zhai, C. Liu, W. Q. Deng and H. Wu, *J. Energy Chem.*, 2023, **76**, 368–376.
62 Q. Zhao, Q. Zhu, J. Miao, P. Zhang and B. Xu, *Nanoscale*, 2019, **11**, 8442–8448.
63 X. Zhao, M. Zhu, C. Tang, K. Quan, Q. Tong, H. Cao, J. Jiang, H. Yang and J. Zhang, *J. Colloid Interface Sci.*, 2022, **620**, 478–485.
64 B. Yang, B. Liu, J. Chen, Y. Ding, Y. Sun, Y. Tang and X. Yan, *Chem. Eng. J.*, 2022, **429**, 132392.

65 P. Yu, G. Cao, S. Yi, X. Zhang, C. Li, X. Sun, K. Wang and Y. Ma, *Nanoscale*, 2018, **10**, 5906–5913.
66 S. Iravani and R. S. Varma, *Mater. Adv.*, 2023, **4**, 4317–4332.
67 K. Das and D. Majumdar, *J. Electroanal. Chem.*, 2022, **905**, 115973.
68 Z. Fan, Y. Wang, Z. Xie, D. Wang, Y. Yuan, H. Kang, B. Su, Z. Cheng and Y. Liu, *Adv. Sci.*, 2018, **5**, 1800750.
69 K. Ghosh and M. Pumera, *Small Methods*, 2021, **5**, 2100451.
70 W. Yang, J. Yang, J. J. Byun, F. P. Moissinac, J. Xu, S. J. Haigh, M. Domingos, M. A. Bissett, R. A. W. Dryfe and S. Barg, *Adv. Mater.*, 2019, **31**, 1902725.
71 M. Yuan, L. Wang, X. Liu, X. Du, G. Zhang, Y. Chang, Q. Xia, Q. Hu and A. Zhou, *Chem. Eng. J.*, 2023, **451**(part 3), 138686.
72 J. Patdiya and B. Kandasubramanian, *Polym.-Plast. Technol. Mater.*, 2021, **60**, 1845–1883.
73 S. Iravani, *Soft Matter*, 2023, **19**, 6196–6212.
74 Y. Wang, T. Guo, Z. Tian, L. Shi, S. C. Barman and H. N. Alshareef, *Matter*, 2023, **6**, 2807–2833.
75 M. Ramezani and Z. M. Ripin, *J. Funct. Biomater.*, 2023, **14**, 347.
76 K. Li, J. Zhao, A. Zhussupbekova, C. E. Shuck, L. Hughes, Y. Dong, S. Barwich, S. Vaesen, I. V. Shvets, M. Möbius, W. Schmitt, Y. Gogotsi and V. Nicolosi, *Nat. Commun.*, 2022, **13**, 6884.
77 P. E. Antezana, S. Municoy, G. Ostapchuk, P. N. Catalano, J. G. Hardy, P. A. Evelson, G. Orive and M. F. Desimone, *Pharmaceutics*, 2023, **15**, 2743.
78 A. Mahmood, T. Akram, C. Shenggui and H. Chen, *Composites, Part B*, 2023, **266**, 110952.
79 S. Mallakpour, F. Tabesh and C. M. Hussain, *Adv. Colloid Interface Sci.*, 2021, **294**, 102482.
80 S. Wang, W. Y. Wu, J. C. C. Yeo, X. Y. D. Soo, W. Thitsartarn, S. Liu, B. H. Tan, A. Suwardi, Z. Li, Q. Zhu and X. J. Loh, *BMEMat*, 2023, **1**, e12021.
81 B. Anasori, M. R. Lukatskaya and Y. Gogotsi, *Nat. Rev. Mater.*, 2017, **2**, 16098.
82 M. L. Matias, C. Pereira, H. V. Almeida, S. Jana, S. Panigrahi, U. D. Menda, D. Nunes, E. Fortunato, R. Martins and S. Nandy, *Mater. Today Adv.*, 2024, **23**, 100512.
83 K. Huang, Z. Li, J. Lin, G. Han and P. Huang, *Chem. Soc. Rev.*, 2018, **47**, 5109–5124.
84 A. Koyappayil, S. G. Chavan, Y. G. Roh and M. H. Lee, *Biosensors*, 2022, **12**, 454.
85 Q. Yi, X. Pei, P. Das, H. Qin, S. W. Lee and R. Esfandyarpour, *Nano Energy*, 2022, **101**, 107511.
86 Z. Li, D. Feng, B. Li, D. Xie and Y. Mei, *Compos. Sci. Technol.*, 2023, **231**, 109803.
87 X. Li, R. Sun, J. Pan, Z. Shi, J. Lv, Z. An, Y. He, Q. Chen, R. P. S. Han, F. Zhang, Y. Lu, H. Liang and Q. Liu, *Small*, 2023, **19**, 2207889.
88 J. Orangi, F. Hamade, V. A. Davis and M. Beidaghi, *ACS Nano*, 2020, **14**, 640–650.
89 S. Zheng, H. Wang, P. Das, Y. Zhang, Y. Cao, J. Ma, S. Liu and Z.-S. Wu, *Adv. Mater.*, 2021, **33**, 2005449.
90 X. Wang, Y. Yu, C. Yang, L. Shang, Y. Zhao and X. Shen, *Adv. Sci.*, 2022, **9**, 2201155.
91 Y. Tan, H. Sun, Y. Lan, H. M. Khan, H. Zhang, L. Zhang, F. Zhang, Y. Cui, L. Zhang, D. Huang, X. Chen, C. Zhou, J. Sun and X. Zhou, *J. Mater. Chem. B*, 2024, **12**, 2158–2179.
92 S. R. A. Ruth, V. R. Feig, H. Tran and Z. Bao, *Adv. Funct. Mater.*, 2020, **30**, 2003491.
93 Z.-H. Tang, Y.-Q. Li, P. Huang, H. Wang, N. Hu and S. Y. Fu, *Compos. Sci. Technol.*, 2021, **208**, 108761.
94 A. Frutiger, J. T. Muth, D. M. Vogt, Y. Mengüç, A. Campo, A. D. Valentine, C. J. Walsh and J. A. Lewis, *Adv. Mater.*, 2015, **27**, 2440–2446.
95 K. Shi, H. Zou, B. Sun, P. Jiang, J. He and X. Huang, *Adv. Funct. Mater.*, 2020, **30**, 1904536.
96 Z. Li, B. Li, B. Chen, J. Zhang and Y. Li, *Nanotechnology*, 2021, **32**, 395503.
97 J. Fu, S. E. Taher, R. K. Abu Al-Rub, T. Zhang, V. Chan and K. Liao, *Adv. Eng. Mater.*, 2022, **24**, 2101388.
98 T. Yang and T. V. Duncan, *Nat. Nanotechnol.*, 2021, **16**, 251–265.
99 K. Vong, S. Eda, Y. Kadota, I. Nasibullin, T. Wakatake, S. Yokoshima, K. Shirasu and K. Tanaka, *Nat. Commun.*, 2019, **10**, 5746.
100 Y. Shao, L. Wei, X. Wu, C. Jiang, Y. Yao, B. Peng, H. Chen, J. Huangfu, Y. Ying, C. J. Zhang and J. Ping, *Nat. Commun.*, 2022, **13**, 3223.
101 H. Liu, C. Du, L. Liao, H. Zhang, H. Zhou, W. Zhou, T. Ren, Z. Sun, Y. Lu, Z. Nie, F. Xu, J. Zhu and W. Huang, *Nat. Commun.*, 2022, **13**, 3420.
102 C. Zhang, Y. Wang, Y. Chang, W. Guo, P. Li, X. Qiao and Z. Yang, *Microchem. J.*, 2024, **200**, 110246.
103 A. P. Tiwari, S. S. Panicker, J. E. Huddy, M. S. Rahman, K. R. Hixon and W. J. Scheideler, *Adv. Mater. Technol.*, 2024, **9**, 2301517.
104 S. Pyo, K. Lee, T. Noh, E. Jo and J. Kim, *Sens. Actuators, B*, 2019, **288**, 618–624.
105 Y. Wang, R. Xu, L. Chen, C. Wu, L. Qiu, C. D. Windle, Q. Han and L. Qu, *ACS Appl. Mater. Interfaces*, 2020, **12**, 8547–8554.
106 P. Puthongkham and B. J. Venton, *ACS Sens.*, 2019, **4**, 2403–2411.
107 A. Zhao, J. She, C. Xiao, J. Xi, Y. Xu, D. Manoj, Y. Sun and F. Xiao, *Sens. Actuators, B*, 2021, **335**, 129683.
108 A. K. Thabit, D. F. Fatani, M. S. Bamakhrama, O. A. Barnawi, L. O. Basudan and S. F. Alhejaili, *Int. J. Infect. Dis.*, 2019, **81**, 128–136.
109 J. Wang, N. He, J. Fei, Z. Ma, Z. Ji, Z. Chen, N. Nie and Y. Huang, *J. Power Sources*, 2022, **551**, 232190.
110 Q. Zhang, Z. Zhang, Q. Liang, F. Gao, F. Yi, M. Ma, Q. Liao, Z. Kang and Y. Zhang, *Nano Energy*, 2019, **55**, 151–163.
111 A. Thakur and P. Devi, *Nano Energy*, 2022, **94**, 106927.
112 J. Nan, X. Guo, J. Xiao, X. Li, W. Chen, W. Wu, H. Liu, Y. Wang, M. Wu and G. Wang, *Small*, 2021, **17**, 1902085.
113 B. Li, J. Zheng, H. Zhang, L. Jin, D. Yang, H. Lv, C. Shen, A. Shellikeri, Y. Zheng, R. Gong, J. P. Zheng and C. Zhang, *Adv. Mater.*, 2018, **30**, 1705670.
114 P. Selinis and F. Farmakis, *J. Electrochem. Soc.*, 2022, **169**, 010526.

115 H. Cha, J. Kim, Y. Lee, J. Cho and M. Park, *Small*, 2018, **14**, 1702989.
116 L. Zhao, B. Ding, X. Y. Qin, Z. Wang, W. Lv, Y. B. He, Q. H. Yang and F. Kang, *Adv. Mater.*, 2022, **34**, 2106704.
117 Q. Tang, Z. Zhou and P. Shen, *J. Am. Chem. Soc.*, 2012, **134**, 16909–16916.
118 Z. Chen, I. Belharouak, Y. K. Sun and K. Amine, *Adv. Funct. Mater.*, 2013, **23**, 959–969.
119 Y. Xie, M. Naguib, V. N. Mochalin, M. W. Barsoum, Y. Gogotsi, X. Yu, K. W. Nam, X. Q. Yang, A. I. Kolesnikov and P. R. C. Kent, *J. Am. Chem. Soc.*, 2014, **136**, 6385–6394.
120 P. Yu, G. Cao, S. Yi, X. Zhang, C. Li, X. Sun, K. Wang and Y. Ma, *Nanoscale*, 2018, **10**, 5906–5913.
121 A. Byeon, A. M. Glushenkov, B. Anasori, P. Urbankowski, J. Li, B. W. Byles, B. Blake, K. L. Van Aken, S. Kota, E. Pomerantseva, J. W. Lee, Y. Chen and Y. Gogotsi, *J. Power Sources*, 2016, **326**, 686–694.
122 J. Li, N. Kurra, M. Seredych, X. Meng, H. Wang and Y. Gogotsi, *Nano Energy*, 2019, **56**, 151–159.
123 M. Beidaghi and Y. Gogotsi, *Energy Environ. Sci.*, 2014, **7**, 867–884.
124 N. A. Kyeremateng, T. Brousse and D. Pech, *Nat. Nanotechnol.*, 2017, **12**, 7–15.
125 X. Kuang, D. J. Roach, J. Wu, C. M. Hamel, Z. Ding, T. Wang, M. L. Dunn and H. J. Qi, *Adv. Funct. Mater.*, 2019, **29**, 1805290.
126 J. Zhang, D. Sun, B. Zhang, Q. Sun, Y. Zhang, S. Liu, Y. Wang, C. Liu, J. Chen, J. Chen, Y. Song and X. Liu, *Mater. Horiz.*, 2022, **9**, 1045–1056.
127 A. S. Kuenstler, Y. Chen, P. Bui, H. Kim, A. DeSimone, L. Jin and R. C. Hayward, *Adv. Mater.*, 2020, **32**, 2000609.
128 B. Cui, M. Ren, L. Dong, Y. Wang, J. He, X. Wei, Y. Zhao, P. Xu, X. Wang, J. Di and Q. Li, *ACS Nano*, 2023, **17**, 12809–12819.
129 Y. Wang, A. Dang, Z. Zhang, R. Yin, Y. Gao, L. Feng and S. Yang, *Adv. Mater.*, 2020, **32**, 2004270.
130 Y. Yang, L. Meng, J. Zhang, Y. Gao, Z. Hao, Y. Liu, M. Niu, X. Zhang, X. Liu and S. Liu, *Adv. Sci.*, 2024, **11**, 2307862.
131 A. D. Auguste, J. W. Ward, J. O. Hardin, B. A. Kowalski, T. C. Guin, J. D. Berrigan and T. J. White, *Adv. Mater.*, 2018, **30**, 1802438.
132 M. O. Saed, W. Elmadih, A. Terentjev, D. Chronopoulos, D. Williamson and E. M. Terentjev, *Nat. Commun.*, 2021, **12**, 6676.
133 J. Zhang, S. Liu, X. Wang, X. Zhang, X. Hu, L. Zhang, Q. Sun and X. Liu, *Mater. Horiz.*, 2024, **11**, 2483–2493.
134 A. Bigham, F. Foroughi, E. Rezvani Ghomi, M. Rafienia, R. E. Neisiany and S. Ramakrishna, *Bio-Des. Manuf.*, 2020, **3**, 281–306.
135 M. Ly, S. Spinelli, S. Hays and D. Zhu, *Eng. Regen.*, 2022, **3**, 41–52.
136 M. Shakiba, E. Rezvani Ghomi, F. Khosravi, S. Jouybar, A. Bigham, M. Zare, M. Abdouss, R. Moaref and S. Ramakrishna, *Polym. Adv. Technol.*, 2021, **32**, 3368–3383.
137 S. Li, B. Gu, X. Li, S. Tang, L. Zheng, E. Ruiz-Hitzky, Z. Sun, C. Xu and X. Wang, *Adv. Healthcare Mater.*, 2022, **11**, 2102367.
138 H. Chen, Y. Cheng, J. Tian, P. Yang, X. Zhang, Y. Chen, Y. Hu and J. Wu, *Sci. Adv.*, 2020, **6**, eaba4311.
139 H. Marks, A. Bucknor, E. Roussakis, N. Nowell, P. Kamali, J. P. Cascales, D. Kazei, S. J. Lin and C. L. Evans, *Sci. Adv.*, 2020, **6**, eabd1061.
140 Y. Esmaeili, A. Farazin, I. Rahimmanesh and A. Bigham, in *Carrier-mediated Gene and Drug Delivery for Dermal Wound Healing*, ed. P. Makvandi and E. N. Zare, Royal Society of Chemistry, 2023, pp. 170–192.
141 M. Shakiba, P. Jahangiri, E. Rahmani, S. M. Hosseini, A. Bigham, A. Foroozandeh, A. Tajiki, M. Pourmadadi, S. Nasiri, S. Jouybar and M. Abdouss, *ACS Appl. Polym. Mater.*, 2023, **5**, 5662–5675.
142 M. Shakiba, M. Sheikhi, Z. Pahnavar, A. Tajiki, A. Bigham, A. Foroozandeh, S. Darvishan, M. Pourmadadi, H. Emadi, J. Rezatabar, H. Abdouss and M. Abdouss, *Int. J. Pharm.*, 2023, **642**, 123207.
143 P. Makvandi, R. Jamaledin, G. Chen, Z. Baghbantaraghdari, E. N. Zare, C. Di Natale, V. Onesto, R. Vecchione, J. Lee, F. R. Tay, P. Netti, V. Mattoli, A. Jaklenec, Z. Gu and R. Langer, *Mater. Today*, 2021, **47**, 206–222.
144 Y. Shao, K. Dong, X. Lu, B. Gao and B. He, *ACS Appl. Mater. Interfaces*, 2022, **14**, 56525–56534.
145 D. Chawla, T. Kaur, A. Joshi and N. Singh, *Int. J. Biol. Macromol.*, 2020, **144**, 560–567.
146 Y. Li, Y. Chen, T. Gan, B. Qin, X. Liu and H. Zhang, *Int. Orthop.*, 2021, **45**, 3033–3043.
147 A. Bigham, M. G. Raucci, K. Zheng, A. R. Boccaccini and L. Ambrosio, *Adv. Mater.*, 2023, 2302858.
148 Z. Li, T. Du, C. Ruan and X. Niu, *Bioact. Mater.*, 2021, **6**, 1491–1511.
149 E. Zeimaran, S. Pourshahrestani, A. Fathi, N. A. B. A. Razak, N. A. Kadri, A. Sheikhi and F. Baino, *Acta Biomater.*, 2021, **136**, 1–36.
150 D. K. Khajuria, V. B. Kumar, D. Gigi, A. Gedanken and D. Karasik, *ACS Appl. Mater. Interfaces*, 2018, **10**, 19373–19385.
151 X. Qu, Y. Guo, C. Xie, S. Li, Z. Liu and B. Lei, *ACS Nano*, 2023, **17**, 7229–7240.
152 H. J. Jo, M. S. Kang, H. J. Heo, H. J. Jang, R. Park, S. W. Hong, Y. H. Kim and D.-W. Han, *Int. J. Biol. Macromol.*, 2024, **265**, 130696.
153 D. M. Henkel, B. J. Witt, B. J. Gersh, S. J. Jacobsen, S. A. Weston, R. A. Meverden and V. L. Roger, *Am. Heart J.*, 2006, **151**, 806–812.
154 H. Esmaeili, A. Patino-Guerrero, M. Hasany, M. O. Ansari, A. Memic, A. Dolatshahi-Pirouz and M. Nikkhah, *Acta Biomater.*, 2022, **139**, 118–140.
155 M. Ghovvati, M. Kharaziha, R. Ardehali and N. Annabi, *Adv. Healthcare Mater.*, 2022, **11**, 2200055.
156 G. Basara, M. Saeidi-Javash, X. Ren, G. Bahcecioglu, B. C. Wyatt, B. Anasori, Y. Zhang and P. Zorlutuna, *Acta Biomater.*, 2022, **139**, 179–189.
157 M. Kansara, M. W. Teng, M. J. Smyth and D. M. Thomas, *Nat. Rev. Cancer*, 2014, **14**, 722–735.
158 A. Bigham, I. Fasolino, S. Borsacchi, C. Valente, L. Calucci, G. Turacchio, M. Pannico, M. Serrano-Ruiz, L. Ambrosio and M. G. Raucci, *Bioact. Mater.*, 2024, **35**, 99–121.

159 D. An, J. Fu, B. Zhang, N. Xie, G. Nie, H. Ågren, M. Qiu and H. Zhang, *Adv. Funct. Mater.*, 2021, **31**, 2101625.
160 M. Ansari, A. Bigham, S. A. Hassanzadeh Tabrizi and H. Abbastabar Ahangar, *J. Am. Ceram. Soc.*, 2018, **101**, 3649–3661.
161 A. Bigham, A. H. Aghajanian, S. Behzadzadeh, Z. Sokhani, S. Shojaei, Y. Kaviani and S. A. Hassanzadeh-Tabrizi, *Mater. Sci. Eng., C*, 2019, **99**, 83–95.
162 A. Bigham, A. H. Aghajanian, A. Saudi and M. Rafienia, *Mater. Sci. Eng., C*, 2020, **109**, 110579.
163 J. Yin, S. Pan, X. Guo, Y. Gao, D. Zhu, Q. Yang, J. Gao, C. Zhang and Y. Chen, *Nano-Micro Lett.*, 2021, **13**, 1–18.
164 H. K. Pektas, Y. Demidov, A. Ahvan, N. Abie, V. S. Georgieva, S. Chen, S. Farè, B. Brachvogel, S. Mathur and H. Maleki, *ACS Mater. Au*, 2023, **3**, 711–726.
165 S. Pan, J. Yin, L. Yu, C. Zhang, Y. Zhu, Y. Gao and Y. Chen, *Adv. Sci.*, 2020, **7**, 1901511.
166 C. Zhao, W. Liu, M. Zhu, C. Wu and Y. Zhu, *Bioact. Mater.*, 2022, **18**, 383–398.
167 A. Bigham, V. Rahimkhoei, P. Abasian, M. Delfi, J. Naderi, M. Ghomi, F. Dabbagh Moghaddam, T. Waqar, Y. Nuri Ertas, S. Sharifi, N. Rabiee, S. Ersoy, A. Maleki, E. Nazarzadeh Zare, E. Sharifi, E. Jabbari, P. Makvandi and A. Akbari, *Chem. Eng. J.*, 2021, **432**, 134146.
168 K. D. Alder, I. Lee, A. M. Munger, H. K. Kwon, M. T. Morris, S. V. Cahill, J. Back, K. E. Yu and F. Y. Lee, *Bone*, 2020, **141**, 115568.
169 Y. Zhao, H. Kang, Y. Xia, L. Sun, F. Li and H. Dai, *Adv. Healthcare Mater.*, 2024, **13**, 2302879.
170 R. Guo, Y. Tian, Y. Wang and W. Yang, *Adv. Funct. Mater.*, 2017, **27**, 1606398.
171 X. Huang, K. Ren, Z. Chang, Y. Ye, D. Huang, W. Zhao, L. Yang, Y. Dong, Z. Cao and H. Qiao, *Chem. Eng. J.*, 2022, **430**, 132898.
172 Q. Yang, H. Yin, T. Xu, D. Zhu, J. Yin, Y. Chen, X. Yu, J. Gao, C. Zhang, Y. Chen and Y. Gao, *Small*, 2020, **16**, 1906814.
173 S. Ghadiri, S. A. Hassanzadeh-Tabrizi and A. Bigham, *J. Sol-Gel Sci. Technol.*, 2017, **83**, 229–236.
174 D. Mehrabani, A. Khodakaram-Tafti, H. Shaterzadeh-Yazdi, B. Zamiri and M. Omidi, *Dent. Traumatol.*, 2018, **34**, 413–420.
175 C. Rinaldi and M. J. A. Wood, *Nat. Rev. Neurol.*, 2018, **14**, 9–21.
176 L. Luo, Y. He, L. Jin, Y. Zhang, F. P. Guastaldi, A. A. Albashari, F. Hu, X. Wang, L. Wang, J. Xiao, L. Li, J. Wang, A. Higuchi and Q. Ye, *Bioact. Mater.*, 2022, **7**, 2.
177 B. G. Jiang, N. Han, F. Rao, Y. L. Wang, Y. H. Kou and P. X. Zhang, *Chin. Med. J.*, 2017, **130**(24), 2996–2998.
178 J. Brandt, L. B. Dahlin and G. Lundborg, *The Journal of Hand Surgery: British & European*, 1999, vol. 24, pp. 284–290.
179 A. Singh, S. Asikainen, A. K. Teotia, P. A. Shiekh, E. Huotilainen, I. Qayoom, J. Partanen, J. Seppälä and A. Kumar, *ACS Appl. Mater. Interfaces*, 2018, **10**, 43327–43342.
180 Z. Wang, Y. Zheng, L. Qiao, Y. Ma, H. Zeng, J. Liang, Q. Ye, K. Shen, B. Liu, L. Sun and Z. Fan, *Adv. Healthcare Mater.*, 2024, 2401093.
181 M. Spector, *Compr. Biomater. II*, 2017, 1–6, DOI: **10.1016/B978-0-08-100691-7.00145-2**.
182 F. Ruan, R. Liu, K. Wang, J. Zeng and Z. Zuo, *J. Hazard. Mater.*, 2021, **402**, 122875.
183 Y. Liu, X. Wei, X. He, J. Yao, R. Tan, P. Chen, B. Yao, J. Zhou and Z. Yao, *Adv. Funct. Mater.*, 2023, **33**, 2211352.
184 H. Jia, X. Yang, Q.-Q. Kong, L.-J. Xie, Q.-G. Guo, G. Song, L.-L. Liang, J.-P. Chen, Y. Li and C.-M. Chen, *J. Mater. Chem. A*, 2021, **9**, 1180–1191.
185 K. Li, L. Han, J. Zhang and J. Cheng, *Small Struct.*, 2023, **4**, 2300210.
186 K. Li, L. Han, T. Wang, J. Zhang and J. Cheng, *J. Mater. Chem. A*, 2024, **12**, 6302–6317.
187 H. Ding, X. Zhang, Y. Liu and S. Ramakrishna, *Int. J. Adv. Manuf. Technol.*, 2019, **105**, 4633–4649.
188 Z.-Q. Liu, H. Qiu, X. Li and S.-L. Yang, *Chin. J. Mech. Eng.*, 2017, **30**, 1447–1459.
189 X. Zhang, R. Nie, Y. Chen and B. He, *J. Elast.*, 2021, **146**, 199–235.
190 Y. Xia, Y. He, F. Zhang, Y. Liu and J. Leng, *Adv. Mater.*, 2021, **33**, 2000713.
191 K. McLellan, T. Li, Y.-C. Sun, M. B. Jakubinek and H. E. Naguib, *ACS Appl. Polym. Mater.*, 2022, **4**, 8774–8785.
192 R. Sajjad, S. T. Chauhdary, M. T. Anwar, A. Zahid, A. A. Khosa, M. Imran and M. H. Sajjad, *Adv. Ind. Eng. Polym. Res.*, 2024, **7**, 20–36.
193 M. Pivar, U. Vrabič-Brodnjak, M. Leskovšek, D. Gregor-Svetec and D. Muck, *Polymers*, 2024, **16**, 2138.
194 S. Joshi, K. Rawat, C. Karunakaran, V. Rajamohan, A. T. Mathew, K. Koziol, V. K. Thakur and A. S. S. Balan, *Appl. Mater. Today*, 2020, **18**, 100490.
195 E. Redondo and M. Pumera, *Electrochem. Commun.*, 2021, **124**, 106920.
196 A. Haleem, M. Javaid, R. P. Singh and R. Suman, *Adv. Ind. Eng. Polym. Res.*, 2021, **4**, 301–311.
197 Y. Li, R. K. Kankala, A.-Z. Chen and S.-B. Wang, *Nanomaterials*, 2022, **12**, 2862.
198 L. Ren, Z. Wang, L. Ren, C. Xu, B. Li, Y. Shi and Q. Liu, *Composites, Part B*, 2023, **265**, 110959.
199 N. Rabiee and S. Iravani, *Mater. Chem. Horiz.*, 2023, **2**, 171–184.
200 M. K. J. E. Exconde, J. A. A. Co, J. Z. Manapat and E. R. Magdaluyo, *Procedia CIRP*, 2019, **84**, 28–32.
201 F. Demoly, M. L. Dunn, K. L. Wood, H. J. Qi and J.-C. André, *Mater. Des.*, 2021, **212**, 110193.
202 A. Zolfagharian, A. Kaynak, M. Bodaghi, A. Z. Kouzani and S. N. Gharaie, *Appl. Sci.*, 2020, **10**, 3020.
203 S. F. Iftekar, A. Aabid, A. Amir and M. Baig, *Polymers*, 2023, **15**, 2519.
204 M. A. Zaed, K. H. Tan, N. Abdullah, R. Saidur, A. K. Pandey and A. M. Saleque, *Open Ceram.*, 2024, **17**, 100526.
205 C. E. Shuck and Y. Gogotsi, *Chem. Eng. J.*, 2020, **401**, 125786.
206 M. Shuaib, A. Haleem, S. Kumar and M. Javaid, *Sustain. Oper. Comput.*, 2021, **2**, 57–63.
207 M. Ramezani and Z. Mohd Ripin, *J. Funct. Biomater.*, 2023, **14**, 347.

